FFI-RAPPORT

20/01912

Introduction to shock-response spectra

Øyvind Andreassen

Introduction to shock-response spectra

Øyvind Andreassen

Norwegian Defence Research Establishment (FFI) 21 November 2020

Keywords
Sjokkrespons-analyse
Sårbarhetsanalyse
Kjøretøy
Marinefartøy

FFI report
20/01912

Project number
144701

Electronic ISBN
978-82-494-3257-1

Approvers
Hanne Bjørk, *Research Director*
Bendik Sagsveen & Anders Helgeland, *Research Manager*

The document is electronically approved and therefore has no handwritten signature.

Copyright
© Norwegian Defence Research Establishment (FFI). The publication may be freely cited where the source is acknowledged.

Summary

A shock is a sudden and violent event. There are many examples of shocks, from earth quakes and explosions to controlled mechanical transient processes. In this report, we discuss theory, modeling and analysis methods of shock response which is how objects respond to shocks. The topic shock response is applicable to buildings, vehicles and ships and a variety of objects that can be exposed to transient forces. It is also applicable to equipment attached to these objects.

Engineers have been working with shocks and transient processes for many years, in particular within the international defence and space sector where the topic is mature and well understood. For example, equipment must be tested and qualified for certain shocks and vibrations before it is installed in a space vehicle and launched into space. The equipment must withstand tests defined according to a certain shock response spectrum. The same applies for equipment used in military vehicles.

We experience that knowledge about shock response and shock response spectra in particular the theoretical side of it, is not so well established among Norwegian defence experts, which is the reason for writing this report. The capability to perform shock simulation and testing, shock analysis and interpretation is essential for and requested by the Armed Forces. Equipment in naval ships and vehicles must withstand certain defined impacts that should be verified and tested before the equipment is purchased and installed.

The main focus of this report is to present and explain the shock response spectrum, why it is useful, how to calculate it and some examples of its use. We also explain how shock response spectrum can be used as design criteria and how they are used in the characterization of shocks. Finally, the “shock spectrum dip” is discussed.

Sammendrag

Sjokk er en voldsom og plutselig hendelse. Det er mange eksempler på sjokk, fra jordskjelv og eksplosjoner til mer kontrollerte transiente mekaniske prosesser. I denne rapporten diskuterer vi teori, modellering og analysemetoder for sjokkrespons. Sjokkrespons angir hvordan objekter responderer på sjokk. Fagfeltet sjokkrespons kan anvendes på bygninger, kjøretøy, farkoster og skip og en mengde forskjellige objekter som kan bli utsatt for transiente krefter. Fagfeltet kan også anvendes på utstyr som er montert på slike objekter.

Ingeniører har arbeidet med sjokk og transiente prosesser i mange år. Spesielt er det relevant for forsvars- og romteknologi. I de store internasjonale miljøene er feltet modent og godt forstått. Innen romfartssektoren må utstyr testes og kvalifiseres etter definerte sjokk- og vibrasjonskriterier før det installeres i romfartøy for å bli brakt ut i rommet. Utstyret må tåle tester som er definert ved gitte sjokkrespons-spektra. Det samme gjelder for militært utstyr.

Vi erfarer at kunnskap om sjokkrespons og sjokkrespons-spektra, spesielt den teoretiske siden av dette, ikke er vel etablert blant norske forsvars-eksperter, hvilket er bakgrunnen for denne rapporten. Evnen til og muligheten for å foreta sjokksimulering og testing, sjokkanalyse og tolkning er essensiell for Forsvaret. Det burde være en grunnleggende ferdighet. Utstyr i marinefartøyer og militære kjøretøy må tåle visse definerte påkjenninger og dette burde være verifisert og testet før utstyret anskaffes og installeres.

Hovedfokus i denne rapporten er å presentere og forklare sjokkrespons-spekteret, hvorfor det er nyttig; og hvordan det kan beregnes. Vi presenterer noen eksempler og vi forklarer hvordan et sjokkrespons-spekter kan brukes som design kriterium og hvordan det kan brukes til å karakterisere sjokkpåvirkning. Tilslutt diskuteres fenomenet “sjokkspektrum-dip”.

Contents

Summary 3

Sammendrag 4

1 Introduction 7
1.1 What is SRS? 8

2 Single Degree of Freedom Support Motion model and the Shock Response Spectrum 9
2.1 Commonly considered pulse shapes 10
2.2 Exact solution of the non-damped oscillator equation for a double half-sine impact signal 14
2.3 Double half-sine shock with damping 16
2.4 Calculation of shock response spectrum 17
2.5 Shock response spectrum plotted on a *tripartite* mesh 17
2.6 What about Fourier analysis of shock impact signals? 22

3 Shock on 2DOF systems 24
3.1 The 2DOF system excited by a harmonic force 24
3.2 The free undamped 2DOF system, initial value problem 25
3.3 Forced undamped 2DOF systems, resonances 27
3.4 Numerical solutions of the forced 2DOF system. Harmonic excitation. 29
3.5 Support motion on 2DOF systems 32
3.6 The shock spectrum dip effect 36
3.7 Shock response and the 3DOF system 36

4 The double beam experiment 39

5 Conclusion 42

Appendix

A Analytical solution for the non-damped sDOF system 43

B The Frahm vibration absorber 45

C nDOF equations for support motion 47

D Analysis of 2DOF eigen frequencies 49

E Matlab example: 50

References 53

1 Introduction

Shock response spectra (SRS) was first used to characterize the impact of earthquakes on buildings by Maurice Biot in 1932, see [4] and [5]. SRS has been used to characterize shocks in aerospace and to characterize ballistic and naval shocks and is used to characterize the frequency content of transient acceleration time-series.

In this report, we explain what a SRS is and how it is computed. In addition, we present some cases from the field of mechanical vibration and discuss them in relation to shock response. The report contains some details of the solution of the governing equations of shock response and SRS with purpose of making a simple and explicit introduction to the novice. A comprehensive treatment of both theory and experiments related to shock response arrived recently, see [19]. A shock response primer is given by J. E .Alexander, see [2].

In the field of shock physics it is common to study shock waves in fluids and gases or shocks waves in solids. Shock is understood as a transient nonlinear dynamic phenomenon. Shock in fluids and gases are treated by many authors, for example Whitham, see [23] or in [13]. For description of nonlinear phenomena in elastic media, see for example the monograph by Hiermaier [12]. SRS as explained in this report is related to the response of linear system to shock impacts. Shock response related to wave propagation through mechanical structures and solids have been studied for decades, see for example [10].

The topic shock response is of importance to many fields of engineering. We have all experienced shock from dropped objects on hard ground and collision of objects. Shocks in structures are related to explosions and earth quakes. Under-water explosions are of concern to the Navy both when it comes to the potential damage of ships and must be taken into consideration when designing future ships.

The topic shock response is a subset of the science of vibration. The last is well studied and documented which may be the case since it is connected to the important field of fatigue in constructions. Engineers are not equally familiar with shock response. When it comes to Norway, we lack expertise in the field and we have presently no test cites specialized on shock response. The explanation is likely that although shocks are of military concern, the topic is of only minor concern to the civil society. Several European countries takes this field seriously and in order to support their navies they have established shock test labs, see [1]. Standards for shock testing procedures and documentation for surface ship equipment within NATO are defined in [20]. Shock design criteria for surface ships are presented for example in [17]. A review of the Dynamic Design Analysis Method DDAM is given in [18]. Here, important work of O'Hara et al at Naval Research Laboratories shocks and ship design criteria is summarized.

When it comes to naval applications, shock response is crucial for naval ship design. Detailed design and test criteria have been developed, see for example [7]. We then talk about design shock spectra. Commonly, SRS are based on acceleration data which can be measured or calculated. For ship design, criteria are given for various vessels, zones above or below waterline, and various degree of surviveability. Naval ship structures as well as equipment on board should withstand shocks defined as design shock criteria, see for example [17].

1.1 What is SRS?

A shock is a sudden violent impulse acting on a mechanical object which will lead to a sudden change in the object's state of motion. A SRS is a quantification of maximum magnitude of acceleration, velocity or displacement in a sudden change as a function of frequency. As presented in detail later in this report, the SRS consists of the maximum magnitudes of acceleration that a set of oscillators of disjunct frequencies will obtain when excited by a sudden impulse (the oscillators are so small that they make no impact back to the device that generated the impulse).

It is our goal to quantify the dynamical consequence of shocks acting on various physical objects. The shock can be quantified through a time series of acceleration. Such time series do not show any dependence on frequency. SRS contain frequency information and is derived from time series of acceleration (or velocity) and displays acceleration (or velocity) magnitude as a function of frequency. The SRS is not like a common Fourier spectrum, but is calculated from the maximum magnitude of acceleration of a set of individual (small) oscillators with disjunct frequencies and damping.

When we talk about a spectrum, which shows amplitude or energy represented as a function of frequency, why not use classical Fourer methods for example by calculating the commonly used power spectral density (PSD)? Fourier methods and applications are extensively discussed in [16]. The reason is simply that shock transients are not periodic and Fourier methods are not well suited for analysis of non-periodic series of data. PSD will be polluted by side lobes. The book written by Brandt [6] contains detailed descriptions of signal processing of vibration data. We will later demonstrate this effect by calculating the PSD of a double half-sine transient often used as a standard excitation pulse for SRS analysis.

A common approach/model in the study of the SRS is to use the simple linear single degree of freedom (sDOF) model of supported motion, for details see [21]. The idea is that the shock is manifested as a prescribed motion of the support and the shock response is calculated as the response of a set of "test-oscillators", see figure 2.2 attached to the support by springs and dampers, but with not impact on the object to be support.

The SRS can be accessed through analytical or numerical models, or through physical tests where the objects under test are instrumented by sensors like accelerometers. The shocks can be generated by explosives, shakers of shock test devices which examples are given in [1].

The SRS is a spectral representation of transient time series. It is a useful tool for designers by indicating at which frequency range the impact of the transient has the most severe impact on certain equipment. Designers can use SRS-analysis, if possible, to avoid resonance frequencies within the actual frequency band.

2 Single Degree of Freedom Support Motion model and the Shock Response Spectrum

The shock response spectrum (SRS) is defined by a linear single degree of freedom (SDOF) support motion model presented below, see J. E. Alexander [2], for more details of support motion, see Thomson and Dahleh [21].

Consider a system with mass m, stiffness k and damping factor c attached to a support as shown in figure 2.1.

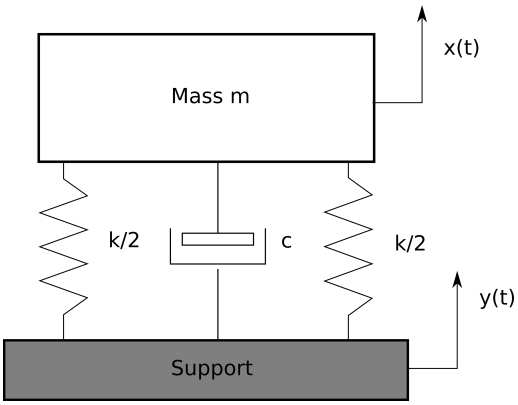

Figure 2.1 Support motion.

The support is brought into motion expressed by time series of acceleration $\ddot{y}(t)$, where the support position is given by $y(t)$ and the position of the "test mass" m is $x(t)$. The separation between mass and support is $z(t) = x(t) - y(t)$. The equation of motion for the mass is

$$m\ddot{x} + c(\dot{x} - \dot{y}) + k(x - y) = 0,$$
$$z = x - y,$$
$$\Downarrow$$
$$\ddot{z} + 2\zeta\omega_n\dot{z} + \omega_n^2 z = -\ddot{y}, \quad \text{where}$$

$\omega_n = \sqrt{k/m}$ is the natural circular frequency and ζ is the damping ratio, $\zeta = c/(2\sqrt{k\,m})$.

The equation of motion for a SDOF support motion forced oscillator is

$$\ddot{z} + 2\zeta\omega_n\dot{z} + \omega_n^2 z = -\ddot{y}. \tag{2.1}$$

From this equation we obtain the acceleration of mass m

$$\ddot{x} = -2\zeta\omega_n\dot{z} - \omega_n^2 z. \tag{2.2}$$

Non-damped oscillations ($c = 0$) are explicitly expressed by the convolution integral

$$z(t) = -\frac{1}{\omega_n}\int_0^t \ddot{y}(\xi)\sin\omega_n(t-\xi)d\xi, \quad \text{and since} \quad \ddot{x}(t) = -\omega_n^2 z(t),$$
$$\ddot{x}(t) = \omega_n\int_0^t \ddot{y}(\xi)\sin\omega_n(t-\xi)d\xi.$$

Mathematically this is a convolution of the support acceleration representing the shock impact on a harmonic oscillator with natural circular frequency ω_n. Both $z(t)$ and $\ddot{x}(t)$ represents the "response" of the shock. Notice that $\ddot{x}(t)$ depends on the oscillator's natural circular frequency ω_n. The corresponding frequency is $f_n = \omega_n/2\pi$.

Now we introduce the SRS and how to calculate it. The process involves the support motion signal $\ddot{y}$ and can be understood as follows:

Consider n nearly massless linear oscillators, which due to their small masses have no impact on the support motion, attached to the support, see figure 2.2. By giving the support an acceleration $\ddot{y}$, these oscillators which we can call *SRS probes* will begin to oscillate at their natural frequencies $f_i = \omega_i/2\pi$, where $\omega_i = \sqrt{(k_i/m)}$. A damping c is assigned to each of the oscillators. Notice that this alters the frequency slightly to $\omega_d = \omega_n\sqrt{1-\zeta^2}$.

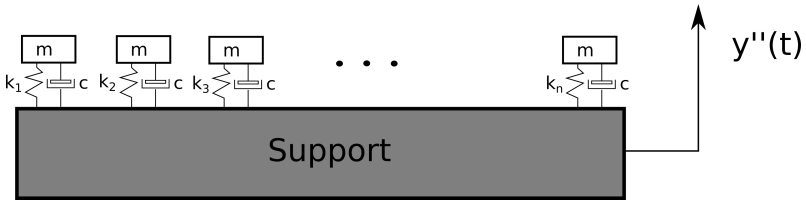

Figure 2.2 Support motion with SRS-probes.

The SRS spectrum is obtained by calculating the maximum magnitude of acceleration $a(f_i) = |\ddot{x}_i|_{\max}$ for each oscillator i, see below. For high frequencies the probes are stiff (k large) and they will follow the motion of the support implying that the SRS values will approach the maximum of the support acceleration. For low frequency the probe stiffness is small and so the acceleration. There are cases where the maximum of acceleration in the SRS is higher than the maximum of the support acceleration $\ddot{y}$. This is called *amplified response* and is due to a resonance of the support motion and the test oscillator.
Technically the SRS is presented on a log-log scale plot. Then for a given input shock/support acceleration $\ddot{y}$, it is common to solve equation (2.1) for a set of oscillators (SRS probes) with frequencies $f_i = \omega_{ni}/2\pi$, over n octaves: $f_i/f_0 = 2^0, 2^1, \ldots, 2^n$. We obtain $n+1$ solutions $\{z_i(t)\}_{i=0}^n$ and from them we calculate the accelerations for each SRS probe $\{\ddot{x}_i(t)\}_{i=0}^n$.
The shock response spectrum is the maximum magnitude over t for each SRS probe $\ddot{x}_i(t)$. It is called **maximax**. The definition of the SRS is

$$a(f_i) = \max\{|\ddot{x}_i(t)|\}, \quad \text{for each} \quad i = 0,, 1, \ldots, n. \tag{2.3}$$

Examples of shock response spectra are shown in figures 2.9 and 2.11.

2.1 Commonly considered pulse shapes

The shock response spectrum can be calculated from idealized pulses with single, double and triple half-sine shapes. It can be calculated from acceleration or velocity time series recorded during tests or from simulation output from various numerical codes, for example structure analysis codes. In physical tests of objects using shakers or shock devices, the shocks must be specified according to certain standards. This can be done by specifying the pulses with maximum acceleration, velocity and displacement or by specifying the shock response spectrum that the test device should deliver. There are many shock profiles used in testing, but the most common are the single, double and triple half-sine profiles. We discuss them in detail below. These profiles can be input as $-\ddot{y}$ in equation (2.1) and the resulting SRS calculated from them.

Half-sine pulse:

The half-sin pulse has amplitude A_1 and width t_1 is defined as

$$a(t) = A_1 \begin{cases} \sin \frac{\pi}{t_1} t, & 0 \leq t \leq t_1, \\ 0, & t_1 < t. \end{cases}$$

For this pulse, the post pulse velocity is $2A_1 t_1/\pi > 0$ which wil impose problems when the base excitation is caused by a shaker. The half-sine pulse is often referred in American literature. Since the post shock velocity is non-zero, the displacement will continue to increase by time.

Haversine pulse:
The haversine pulse is another commonly considered pulse. It is defined as

$$a(t) = \frac{A_1}{2} \begin{cases} 1 - \cos(\frac{2\pi t}{t_1}), & 0 \leq t \leq t_1, \\ 0, & t_1 < t. \end{cases}$$

The post pulse velocity of the haversine is $A_1 t_1/2 < 2A_1 t_1/\pi$ which is smaller than the post pulse velocity for the half-sine pulse. In figure 2.3 the half-sine and haversine pulses are plotted with same amplitude and width. In figure 2.12 the SRSs of the two pulses are shown.

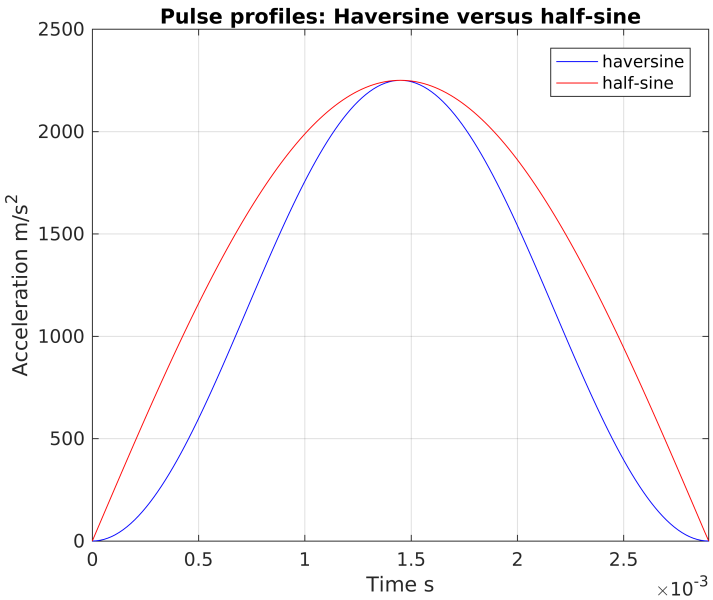

Figure 2.3 Comparison of the half-sine and the haversine pulse.

Double half-sine pulse:
This is a pulse commonly used by the German/Dutch navy and referred in the document [7]. The reason for this is physical. The pulse shape of shocks created by underwater explosions (which in the near field has a closely spherical shape) has first a positive acceleration peak in the expansion phase and a weaker negative acceleration peak in the contraction phase. This is approximated by a double half-sine pulse. A cavitation bubble is formed which oscillates. These oscillations are damped after a few expansions/contractions. This is not considered here, but it is possible to include

shapes of the form $e^{-\alpha t}\sin(\pi t/t_1)$ for the SRS calculation as well. This is considered indirectly in section 3 of this report.

The double half-sine pulse is defined such that the base stops when the pulse has ended. The end position is different from the start position. This limits the use of shakers to pulses where the base motion is small. The double half-sine pulse is constructed such that the velocity reaches zero after the pulse which is possible only if the areas under the first and second pulse are equal: $v(t_2) = \int_0^{t_1} a(t) + \int_{t_1}^{t_2} a(t) = 0$. The following pulse satisfies this condition

$$a(t) = A_1 \begin{cases} \sin\frac{\pi}{t_1}t, & 0 \le t \le t_1, \\ -\frac{t_1}{t_2-t_1}\sin\frac{\pi(t-t_1)}{t_2-t_1}, & t_1 < t \le t_2, \\ 0, & t_2 < t. \end{cases} \tag{2.4}$$

By integrating and double integrating this expression we get the velocity and displacement of the base

$$v(t) = A_1\frac{t_1}{\pi} \begin{cases} 1-\cos\frac{\pi}{t_1}t, & 0 \le t \le t_1, \\ 1+\cos\frac{\pi(t-t_1)}{t_2-t_1}, & t_1 < t \le t_2, \\ 0, & t_2 < t, \end{cases} \tag{2.5}$$

$$y(t) = A_1\frac{t_1}{\pi} \begin{cases} t-\frac{t_1}{\pi}\sin\frac{\pi}{t_1}t, & 0 \le t \le t_1, \\ t+\frac{t_2-t_1}{\pi}\sin\frac{\pi(t-t_1)}{t_2-t_1}, & t_1 < t \le t_2, \\ t_2, & t_2 < t. \end{cases} \tag{2.6}$$

Notice that for the double half-sine pulse, $v(t_2) = 0$,but the end displacement becomes $y(t_2) = A_1 t_1 t_2/\pi$ which is not zero. This has to be taken into account when doing SRS tests using this pulse. Evidently, $a(t), v(t)$ and $y(t)$ are continuous at $t = t_1$ and $t = t_2$.

Assuming a double half-sine accelerated base motion. From the formulas above, it is evident that the base motion can be specified in two equivalent ways. 1) Specifying A_1, A_2, t_1, t_2. Zero motion at the end of the pulse gives $A_2 = -A_1 t_1/(t_2 - t_1)$, leaving A_1, t_1, t_2 as free parameters. We can calculate max values of acceleration $a_0 = A_1$, velocity $v_0 = 2A_1 t_1/\pi$ and displacement $y_0 = A_1 t_1 t_2/\pi$ of this pulse. 2) Contrary, knowing the maximum acceleration, velocity and displacement of the pulse, we can calculate $A_1 = a_0, t_1 = \frac{\pi}{2}\frac{v_0}{a_0}, t_2 = 2\frac{y_0}{v_0}$. The specifications are equivalent

$$\text{Double half-sine pulse: } (A_1, t_1, t_2) \quad \Leftrightarrow \quad (a_0, v_0, d_0).$$

Example:
$A_1 = 2250\,\mathrm{m/s^2}$,
$A_2 = -750\,\mathrm{m/s^2}$,
$t_1 = 0.0029\,\mathrm{s}$,
$t_2 = 0.0116\,\mathrm{s}$,
$t_2 - t_1 = 0.0087\,\mathrm{s}$

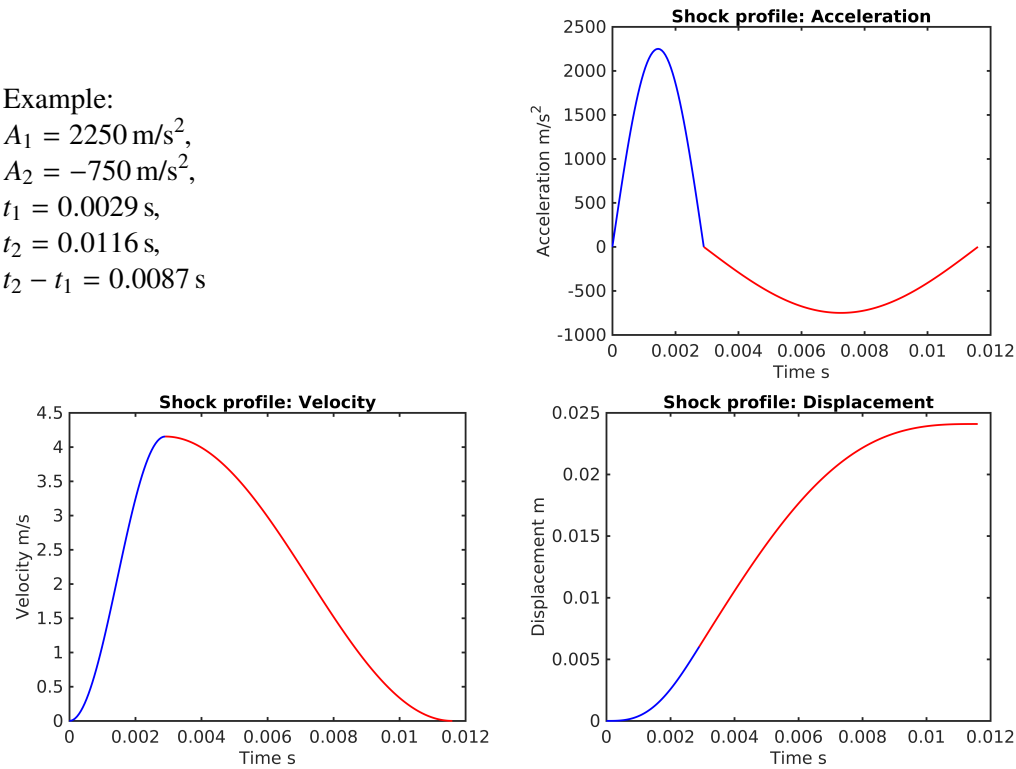

Figure 2.4 Double half-sine shock profile.

The triple pulse:
It is possible also to define a triple-pulse shock with both zero velocity and displacement at the end. This pulse shape is more suited for shakers. The base is withdrawn before and after the pulse. The magnitude of acceleration is somewhat limited by shakers, and in cases of shocks with large accelerations and/or velocity, masses and displacements, other kinds of shock machines may be used. For the triple pulse, the acceleration is

$$a(t) = \begin{cases} A_1 \sin \frac{\pi}{t_1} t, & 0 \le t \le t_1, \\ A_2 \sin \frac{\pi(t-t_1)}{t_2-t_1}, & t_1 < t \le t_2, \\ A_1 \sin \frac{\pi(t-t_2)}{t_3-t_2}, & t_2 < t \le t_3, \\ 0, & t_3 < t. \end{cases}$$

Assuming $A_2 = -2A_1 t_1/(t_2 - t_1)$, and $t_3 - t_2 = t_1$, then

$$v(t) = A_1 \frac{t_1}{\pi} \begin{cases} \cos \frac{\pi}{t_1} t - 1, & 0 \le t \le t_1, \\ -2 \cos \frac{\pi(t-t_1)}{t_2-t_1}, & t_1 < t \le t_2, \\ 1 + \cos \frac{\pi(t-t_2)}{t_3-t_2}, & t_2 < t \le t_3, \\ 0, & t_3 < t, \end{cases}$$

$$y(t) = A_1 \frac{t_1}{\pi} \begin{cases} \frac{t_1}{\pi} \sin \frac{\pi}{t_1} t - t, & 0 \le t \le t_1, \\ -t_1 - \frac{2(t_2 - t_1)}{\pi} \sin \frac{\pi(t - t_1)}{t_2 - t_1}, & t_1 < t \le t_2, \\ t - (t_1 + t_2) + \frac{t_1}{\pi} \sin \frac{\pi(t - t_2)}{t_3 - t_2}, & t_2 < t \le t_3, \\ 0, & t_3 < t, \end{cases}$$

then $v(t_3) = 0$, $y(t_3) = 0$, and $a(t)$, $v(t)$, $y(t)$ are continuous at $t = t_1, t_2, t_3$.

Example:
$A_2 = 2250\,\mathrm{m/s^2}$,
$A_1 = -326\,\mathrm{m/s^2}$,
$t_1 = 0.010\,\mathrm{s}$,
$t_2 = 0.0129\,\mathrm{s}$,
$t_2 - t_1 = 0.0029\,\mathrm{s}$,
$t_3 = t_1 + t_2 = 0.0229\,\mathrm{s}$.

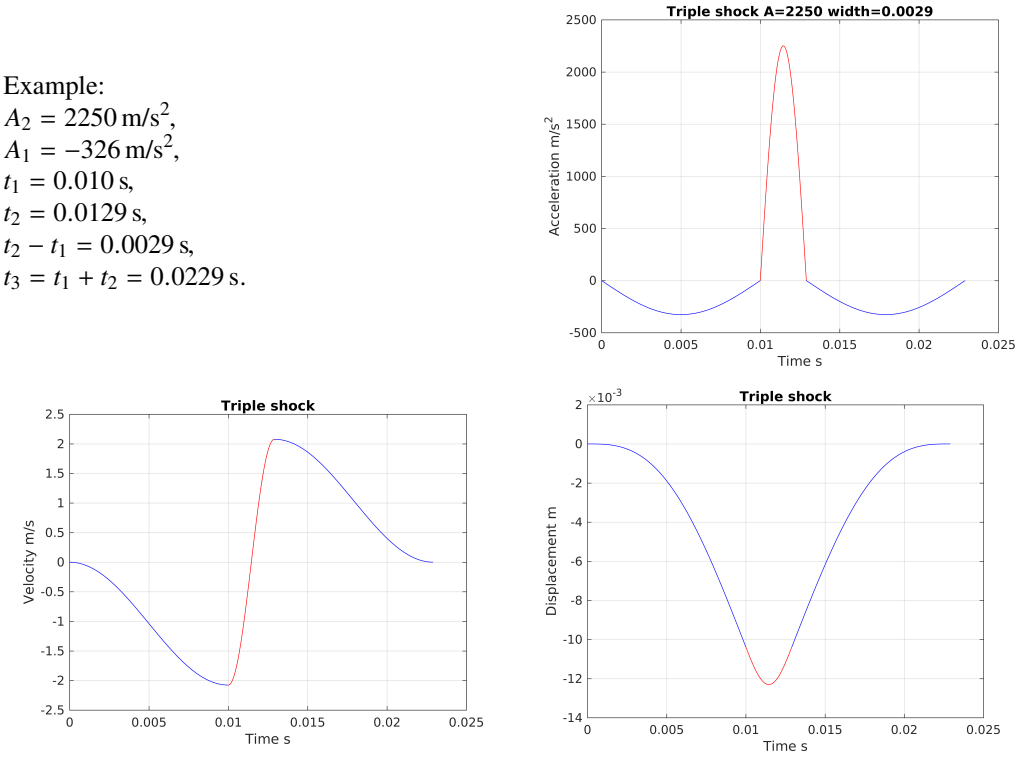

Figure 2.5 Triple half-sine shock profile.

This triple-sine pulse has the same width and peak acceleration as the single and double pulse discussed previously.

2.2 Exact solution of the non-damped oscillator equation for a double half-sine impact signal

The analytic solution is derived mostly for checking the numerical codes developed for treating the SRS cases that follows later in this report, but also for getting a better overview of the behavior of the solutions. Consider the equation for the non-damped base excited oscillator with forcing expressed by (2.4), we have

$$\ddot{z} + \omega_n^2 z = -\ddot{y} = -A_1 \begin{cases} \sin p_1 t, & 0 \le t \le t_1, \\ -\frac{t_1}{t_2 - t_1} \sin p_2 (t - t_1), & t_1 < t \le t_2, \\ 0, & t_2 < t. \end{cases} \tag{2.7}$$

Here $p_1 = (\pi/t_1)$ and $p_2 = \pi/(t_2 - t_1)$, $R_{1,2} = p_{1,2}/\omega_n$, $q = t_1/(t_2 - t_1)$, $K_{1,2} = 1/(1 - (p_{1,2}/\omega_n)^2)$. A detailed description of solving equation 2.7 is given in appendix A. Here we limit ourselves to write up the result

$$z(t) = \begin{cases} (A_1/\omega_n^2)K_1 \left\{R_1 \sin\omega_n t - \sin p_1 t\right\}, & 0 \le t \le t_1, \\ (A_1/\omega_n^2)\left\{(K_1R_1 - K_2R_2q)\sin\omega_n(t-t_1) + \right. & \\ \left. K_1R_1 \sin\omega_n t + K_2 q \sin p_2(t-t_1)\right\}, & 0 \le t \le t_1, \\ A\sin\omega_n(t-t_2) + B\cos\omega_n(t-t_2), & t_2 < t, \end{cases} \tag{2.8}$$

where

$$A = (A_1/\omega_n^2)\left\{(K_1R_1 - K_2R_2q)\cos\omega_n(t_2-t_1) + K_1R_1\cos\omega_n t_2 - K_2R_2q\right\}, \tag{2.9}$$

$$B = (A_1/\omega_n^2)\left\{(K_1R_1 - K_2R_2q)\sin\omega_n(t_2-t_1) + K_1R_1\sin\omega_n t_2\right\}. \tag{2.10}$$

Knowing $\ddot{z}$ or z, we can calculate the acceleration $\ddot{x}$ as follows

$$\ddot{x} = \ddot{y} + \ddot{z} = -\omega_n^2 z. \tag{2.11}$$

Let us take a detailed look the test oscillator signal at frequency 200 Hz, see figure 2.6.

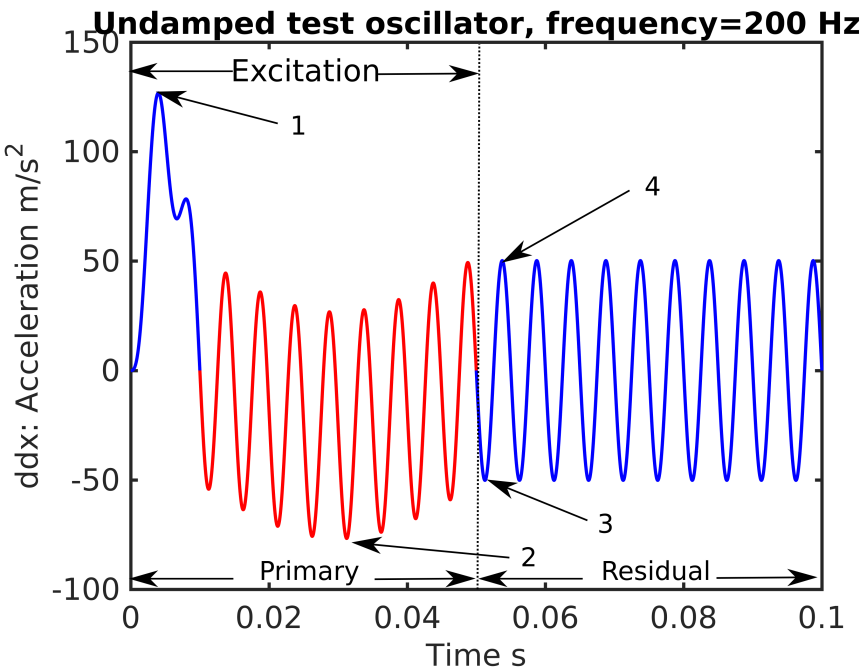

Figure 2.6 *Test oscillator with frequency 200 Hz shocked by a double half-sine pulse with peak acceleration of 100 m/s^2. The signal is divided into a primary where the excitation occurs and a residual part. The numbers 1, . . . , 4 mark as follows: 1-primary maximum positive - maximax, 2-primary maximum negative, 3-residual negative, 4-residual positive. Notice that the test oscillator obtains a peak acceleration that is higher than the exciting pulse. This is called amplified response which is caused by resonance.*

In figure 2.7, accelerations of test oscillators with natural frequencies of 20, 50, 100, 200, 400 Hz are shown.

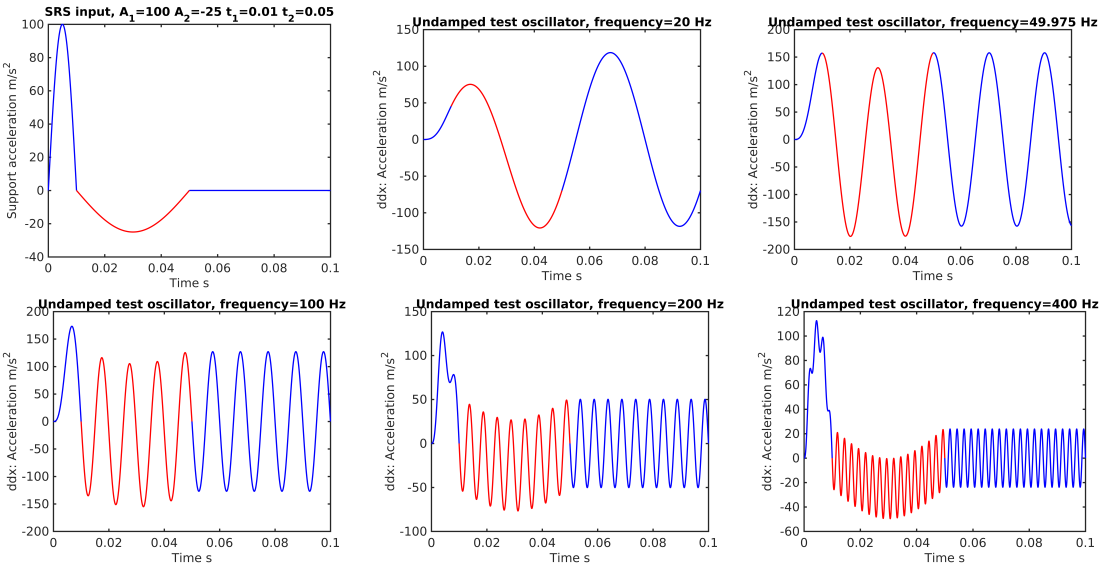

Figure 2.7 Plots of acceleration of the base and base excited non-damped oscillators with natural frequencies $f = 20, 50, 100, 200, 400$ Hz.

We observe that maximum accelerations/retardations of the oscillating mass is larger than the maximum base acceleration (amplified response or resonant amplification). There is an indication that for high frequencies, the maximum acceleration of the mass, approach maximum base acceleration. That is due to the high stiffness at high frequencies. Notice that the max $|\ddot{x}|$ (**maximax**) can occur in the negative part of the signal which is the case for the natural frequency 20 Hz.

2.3 Double half-sine shock with damping

Support motion with damping: We have $z = x - y$, the equation of motion including damping (2.1) is

$$\ddot{z} + 2\zeta\omega_n\dot{z} + \omega_n^2 z = -\ddot{y}.$$

For numerical integration, we write this equation as a set of two first order equations. Introducing $\xi = \dot{z}$ gives

$$\begin{pmatrix}\dot{\xi}\\ \dot{z}\end{pmatrix} = \begin{pmatrix}-2\zeta\omega_n & -\omega_n^2\\ 1 & 0\end{pmatrix}\begin{pmatrix}\xi\\ z\end{pmatrix} + \begin{pmatrix}-\ddot{y}\\ 0\end{pmatrix}. \tag{2.12}$$

This equation is solved with the initial condition

$$\begin{pmatrix}\xi\\ z\end{pmatrix} = \begin{pmatrix}0\\ 0\end{pmatrix}.$$

The solver gives $\dot{z}$ and z. $\ddot{x}$ is calculated from $\ddot{x} = -2\zeta\omega_n\dot{z} - \omega_n^2 z$. The damping ratio ζ is related to the quality factor Q, which is the normalized resonance peak value. It is defined as

$$Q = \frac{1}{2\zeta}, \quad \text{and} \quad \%\text{Cr} = 50/Q.$$

Oscillations are critically damped if $Q = 1/2$, for $Q < 1/2$ they are over-damped. Critical damping occurs when $Q = 1/2, \%\text{Cr} = 100$. For example a damping of 1% relative to critical damping (%Cr = 1) corresponds to $Q = 50$. High quality factor means small damping. Solutions of 2.12 for selected frequencies ω_n are shown in the plots below. We use Matlab with RK45 for the numerical integration.

Some of the oscillators with $Q = 10$ (damping of 5%), shows amplified response. The maximum of the base pulse is 2250 m/s^2, see figure 2.8, and the oscillator with natural frequency of 200 Hz has a maximum at about 3300 m/s^2 implying that the SRS can have values above the maximum base acceleration. We get a view of this phenomenon when we plot the shock response spectrum as is done in the next section.

2.4 Calculation of shock response spectrum

Consider the case presented in last section. We solve equation 2.12 for the double half-sine shock and calculate $\max|\ddot{x}|$ **maximax** for oscillators with natural frequencies covering a range of octaves, for example 10 octaves $\omega_{ni} = 2\pi f_i$, with $f_i = f_0 \cdot 2^i, i = 0, \ldots, 10$. Pseudo-velocity is calculated by the expression $v_i = a_i/(2\pi f_i)$, pseudo displacement is calculated by $d_i = a_i/(2\pi f_i)^2$. A SRS plot is shown in figure 2.9, but by introducing a tripartite mesh (which is constructed as shown in figure 2.10), these three figures can be plotted as a single figure. This is explained in section 2.5 and shown in figure 2.11.

2.5 Shock response spectrum plotted on a *tripartite* mesh

Pseudo-velocity is defined as $v_i = a_i/(2\pi f_i) \Leftrightarrow a_i = 2\pi f_i v_i$. Pseudo-displacement is defined as $d_i = v_i/(2\pi f_i)$. We normalize SRS of acceleration $S_a(f)$ by g. Then SRS of acceleration, velocity and displacement are related as

$$\begin{aligned} S_a(f) &= 2\pi f S_v(f)/g, \\ S_d(f) &= S_v(f)/2\pi f, \end{aligned} \quad \Rightarrow \quad \begin{aligned} \log(S_a(f)) &= \log(2\pi/g) + \log(f) + \log(S_v(f)), \\ \log(S_d(f)) &= -\log(2\pi) - \log(f) + \log(S_v(f)). \end{aligned}$$

Assuming $S_a(f)$ constant, then

$$\log(S_v(f)) = K_1 - \log(f),$$

consists of lines with inclination -1. Assuming constant $S_d(f)$, then

$$\log(S_v(f)) = K_2 + \log(f),$$

consists of lines with inclination $+1$ the coordinate lines will be inclined $\pm 45°$ to the $f = constant$ lines.

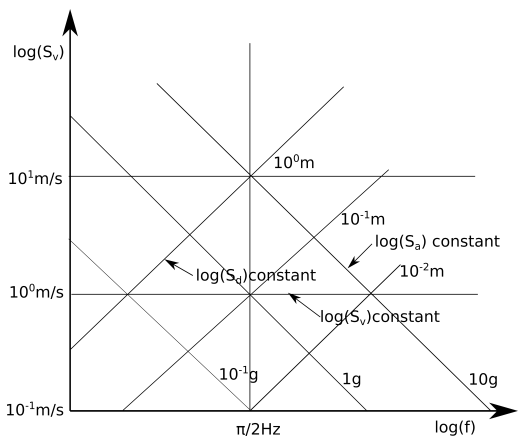

Figure 2.10 Tripartite mesh.

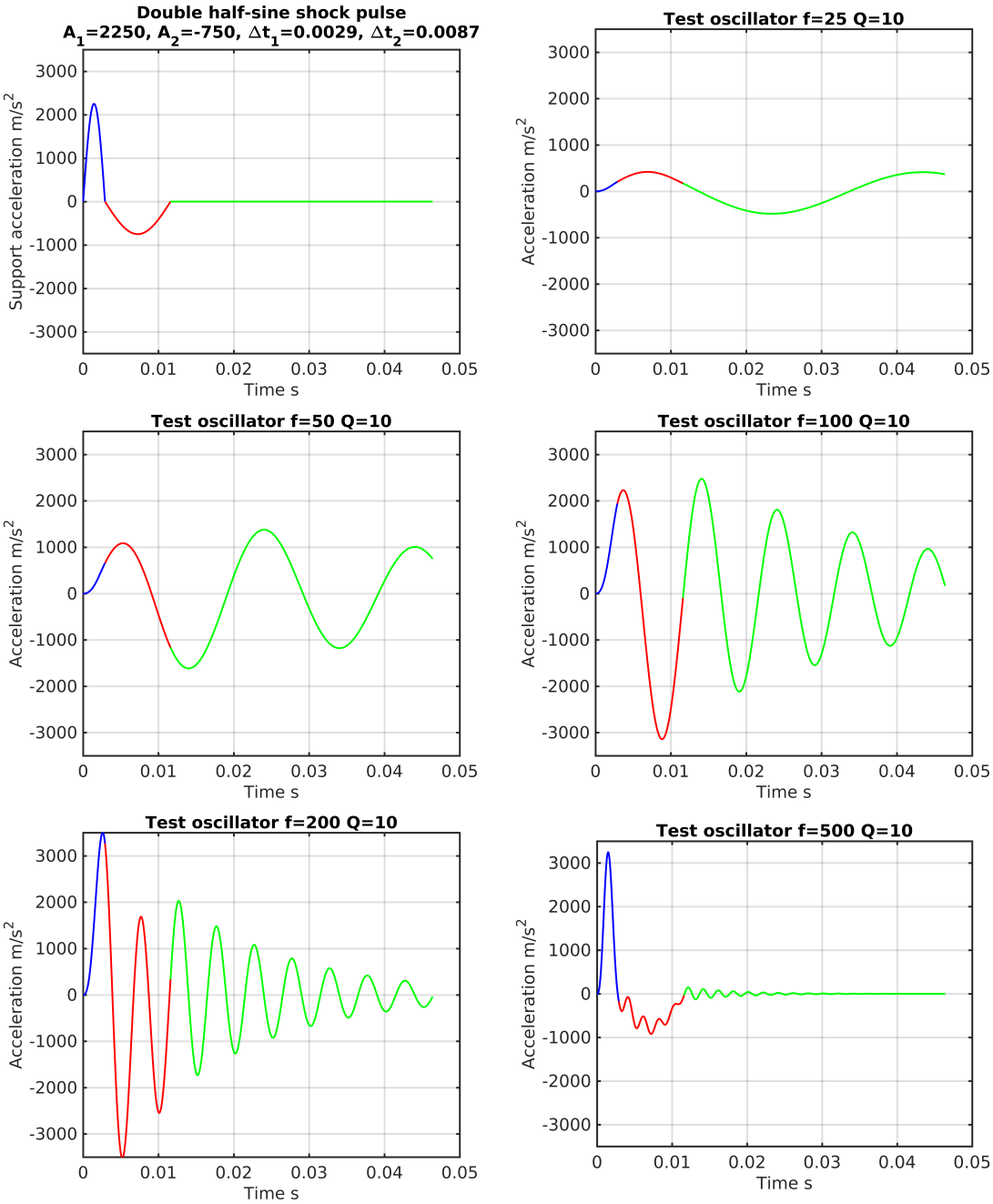

Figure 2.8 *Oscillators excited by a double half-sine pulse as described in figure 2.4. The test oscillators have quality factor* $Q = 10$ *and natural frequencies* $25, 50, 100, 500\,Hz$. *Notice that for oscillators with frequencies above* $100\,Hz$ *also the damped oscillators shows amplified response.*

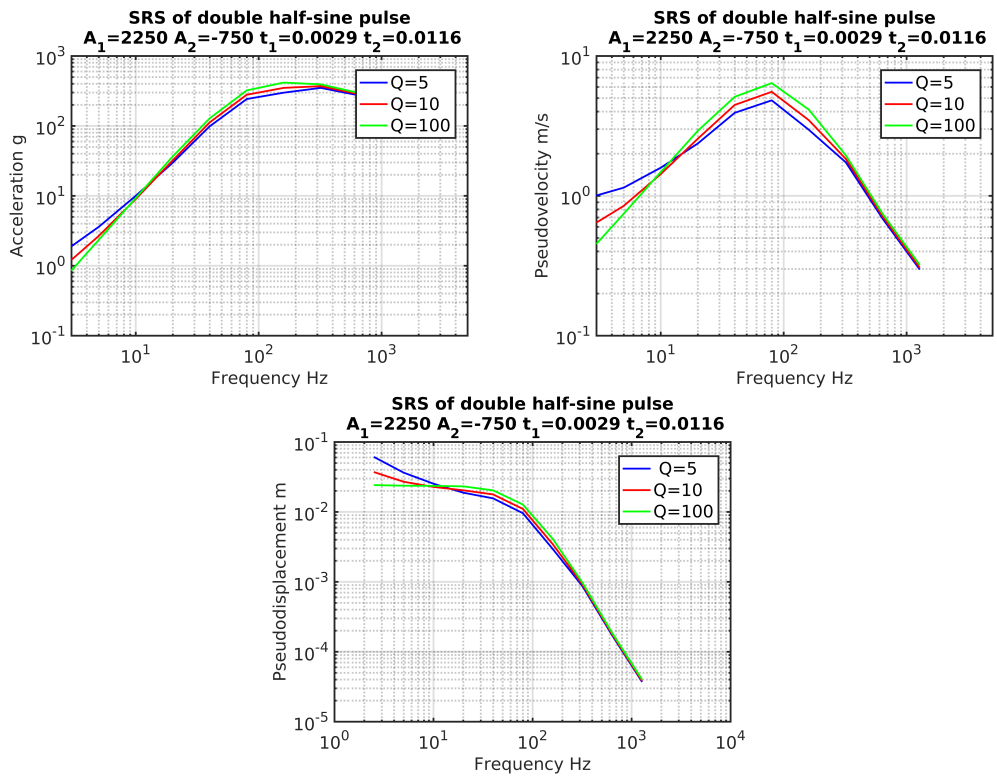

Figure 2.9 SRS of double half-sine shock. Upper left graph shows SRS of acceleration, upper right figure shows SRS of pseudo-velocity, lower figure shows SRS of pseudo-displacement. The spectra are calculated for quality factors $Q = 5, 10, 100$.

Consider the grid lines that cross each other at the point ($\pi/2$ Hz, 10^{-1} m/s). Here S_a is calculated in units of g: $S_a = (2\pi \cdot \pi/2g)S_v \approx 10^{-1}g$, and $S_d = S_v/(2\pi \cdot \pi/2) \approx 10^{-2}$ m. A tripartite SRS plot of the double half-sine pulse previously discussed is shown in figure 2.11, where the three figures shown in figure 2.9 are merged into one. A tripartite plot indicates magnitude of velocity, displacement and acceleration at specified frequencies for a given shock.

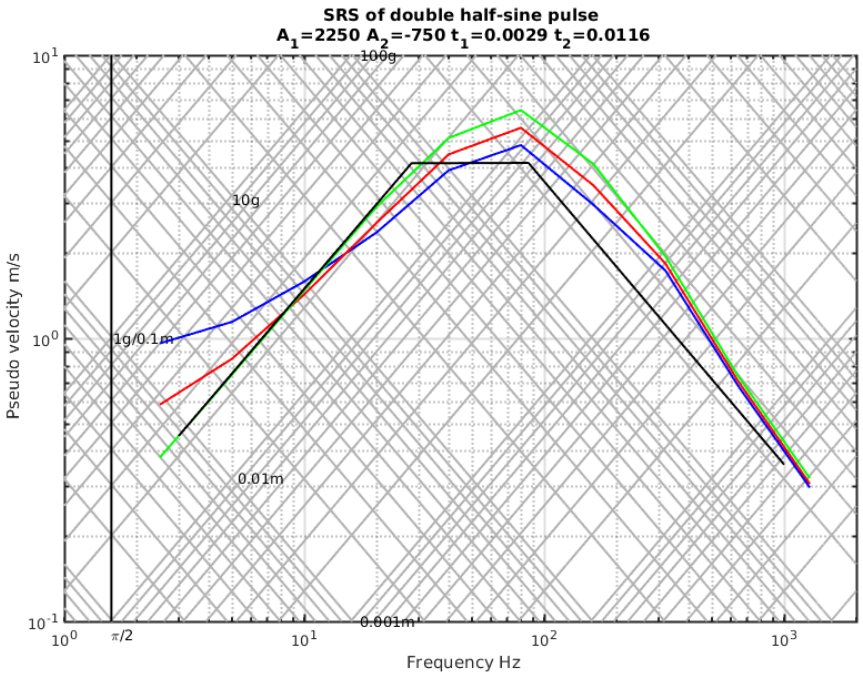

Figure 2.11 *Tripartite plot showing SRS of a double half-sine pulse defined in figure 2.4. These shock values corresponds to max values in the pulse given in acceleration, velocity and displacement as* $(a_0, v_0, d_0) = (225g, 4.154m/s, 0.024m)$. *The black curve shows these values. Notice that parts of the calculated SRS curves are above the black curve which is called region of amplified response. Max acceleration in the SRS is* $400\,g$ *while the peak of the pulse is* $225\,g$. *Blue,red,green curves correspond to* $Q = 5, 10, 100$. *The vertical black line marks* $f = \pi/2$. *The green curve with negligible damping* $Q = 100$, *approach the max displacement* d_0 *for* $f \to 0$ *(low stiffness) and max acceleration* a_0 *for* $f \to \infty$ *(high stiffness). Notice that the curves for high damping* $Q = 5, 10$ *are above the black line for low frequencies. This is due to the force transmitted through the damper.*

Graphs on a tripartite mesh can be used to define shock strengths through d_0, v_0, a_0 as shown by the black curve in figure 2.11. They can also be used to present data from measurements of shocks. They can be calculated from accelerometer data recorded during a shock event, where they give an indication of displacement, velocity and acceleration as a function of frequency. Such curves

are very useful as design criteria for equipment thought to withstand shocks. As an alternative to d_0, v_0, a_0, one can assume something about the nature of the shock for example the shock can be shaped as a double half-sine pulse. Then the numbers A_1, A_2, t_1, t_2 are given. For the double half-sine pulse, these descriptions are equivalent. It is important to notify that this is not generally the case. Time series of a acceleration describing a shock can in most cases not be reproduced from the SRS.

The shock response spectra of a single half-sine and a haversine pulse is shown in figure 2.12 for comparison. As expected the SRS values of single half-sine pulse are higher than for the haversine.

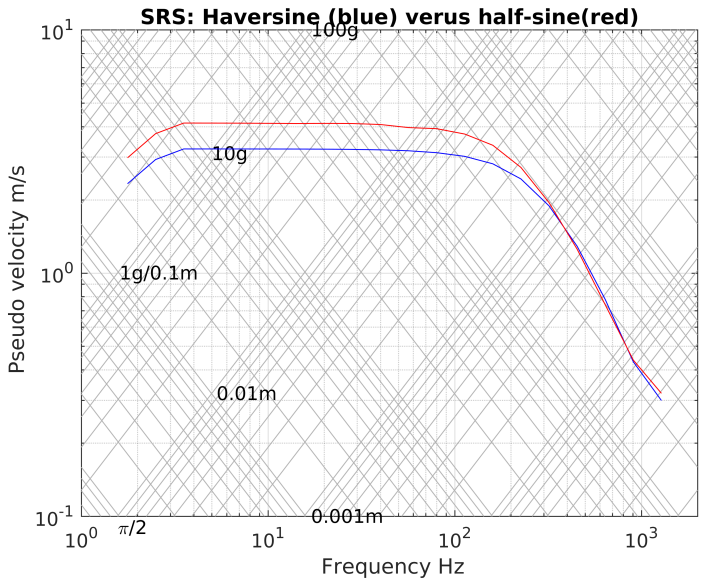

Figure 2.12 SRS of a haversine (red curve) compared with a single half-sine pulse (blue curve). Peak accelerations and pulse widths are $2250\,m/s^2$ *and* $\delta t = 2.9\,ms$, $Q = 100$ *in both cases.*

The shock response spectra of a single half-sine and a double half-sine and a triple half-sine pulse with same peak vales and widths are for comparison shown in figure 2.13. Evidently the single pulse has higher values of pseudo-velocity and pseudo-displacement in the low frequency region of the spectrum. Since the single-pulse never stops, $v = 2At/\pi$ after the shock, the displacement continue to increase with time. Some shock experts have a negative attitude against the use of EM shakers as shock machines, see comments in [19]. One of the reasons is that shakers have to stop after the shock and double or triple pulses must be used.

To obtain the stop in the same position as the start, the piston must be withdrawn prior and after the shock. This reduces velocity and displacement in the low frequency part of the spectrum. Limiting the displacement and velocity of the pulse. For the double pulse, the piston ends in a different position from the start position, limiting the amplitude of the shock. This is even more severe for the triple pulse. From the plots in figure 2.13, we see that the pseudo-velocity and pseudo-displacement in the low frequency part of the spectrum have higher values for the single

pulse than for the two other pulses. However, there are other ways to increase the SRS magnitudes of shakers. That is by superposing series of damped sine functions, making a pulse train with a complex pattern. Because of this, and in addition the limits of mass and acceleration that can be handled by electro-magnetic shakers some engineers are skeptical to the use of such shakers in SRS tests.

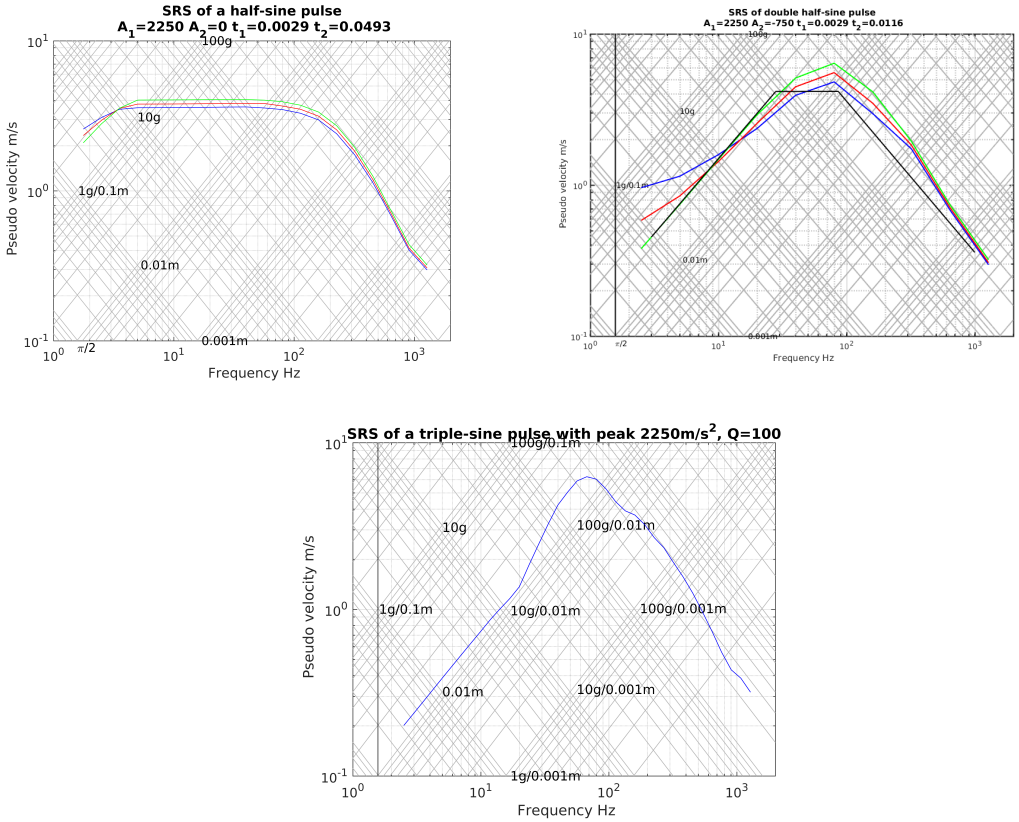

Figure 2.13 *Comparison of SRS of a single, double and triple half-sine pulse with the same peak acceleration $A = 2250\,m/s^2$ and width $\delta t = 2.9\,ms$. The upper left plot shows SRS of a single half-sine pulse, the upper right plot shows the SRS of a double half-sine pulse while the lower plot shows the SRS of a triple half-sine pulse. The blue, red, green curves correspond to $Q = 5, 10, 100$. In the lower plot, $Q = 100$. The double and in particular the triple pulse SRS drops off considerably for low frequencies. This is a drawback when electromagnetic shakers are used to create shocks since they can not simulate a single-sine pulse shocks. The low frequency dip of the single half-sine pulse is caused by limited integration time domain for the ODE integration.*

2.6 What about Fourier analysis of shock impact signals?

Consider the double half-sine shock profile derived in previous section. We calculate Power Spectral Density of the signal, see [22]. The resulting spectrum is strongly affected by side-lobes masking the frequency content of the signal as shown in figure 2.15. The shock signal consists of two half

sines of respectively with "corresponding frequencies" $f_1 = 100\,\text{Hz}$ and $f_2 = 500\,\text{Hz}$. As show in the plot, we do not see any sign of any of them.

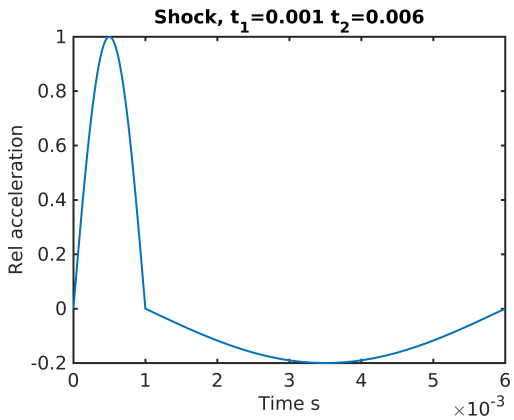

Figure 2.14 Double half-sine shock signal.

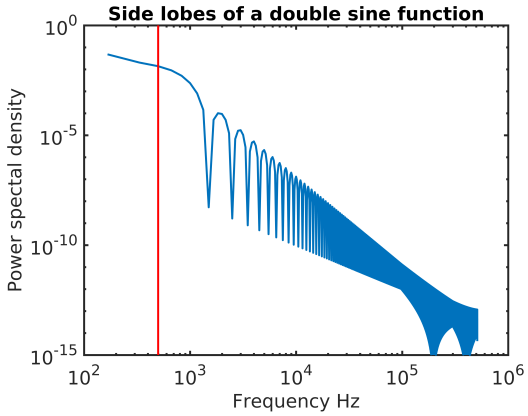

Figure 2.15 Power Spectral density of the double half-sine pulse.

3 Shock on 2DOF systems

2DOF systems consist of two vibrating masses, see figures 3.1 or 3.7. There are two natural frequencies $\omega_1 = \sqrt{k_1/m_1},\ \omega_2 = \sqrt{k_2/m_2}$ and two eigen-frequencies ω_1^*, ω_2^* which are the roots of equation 3.9. The eigen frequencies are generally disjunct. Belonging to the eigen-frequencies are two eigen-vectors which expresses the normal modes of oscillations. The general solution of the problem is a superposition of the normal modes.

A striking phenomena that can appear in 2DOF systems is the dynamic vibration absorber invented by Hermann Frahm in1909, see [8] and [11]. Vibration control of structures including active and passive methods is extensively described in a book edited by Hagedorn and Spelsberg-Korspeter, see [9]. Vibration control should be of great interest to the navy since vibration and sound generation is strongly connected.

Vibration absorption according to Frahn and first theoretically explained by den Hartog [11], is described in section 3.4 and in appendix B. The dynamic vibration absorber consists of a small vibrating element (absorber) which is attached to the main SDOF system which we want to damp. It works when the main system is excited by a harmonic fore and the frequency of the force is the same as the natural frequency of the absorbing element. The shock pulse is broad banded and one can ask whether the damper has a damping effect on shocks. In fact, the dynamic damper causes the shock spectrum dip effect described experimentally in O'Hara in [14] and through a simple model in O'Hara and Cunniff in [15]. We present the theory for the shock spectrum dip below.

3.1 The 2DOF system excited by a harmonic force

A 2DOF model of a medium-weight shock machine is presented by Alexander in [3]. The model consists of two masses connected by a spring and damper (which is strictly a SDOF system when treated in mass-center coordinates). Here we give a general treatment of a 2DOF system consisting of two springs/dampers and two masses. We discuss free vibrations, forced vibrations, the dynamic vibration absorber and finally the 2DOF support motion case.

Consider a system containing masses m_1 and m_2, springs k_1 and k_2 and damping c_1 and c_2 attached to a fixed wall as shown in figure 3.1. A force $F = F_0 e^{i\omega t}$ is applied to m_1. Force balance implies the following equations

$$m_1\ddot{x}_1 = -k_1x_1 - c_1\dot{x}_1 + k_2(x_2 - x_1) + c_2(\dot{x}_2 - \dot{x}_1) + F_0e^{i\omega t}, \tag{3.1}$$

$$m_2\ddot{x}_2 = -k_2(x_2 - x_1) - c_2(\dot{x}_2 - \dot{x}_1). \tag{3.2}$$

By writing $z_1 = x_1$ and $z_2 = x_2 - x_1$, and introducing $\mu = m_2/m_1, 2\zeta_i\omega_i = c_i/m_i, \omega_i^2 = k_i/m_i$, we get

$$\ddot{z}_1 + 2\zeta_1\omega_1\dot{z}_1 + \omega_1^2 z_1 - 2\zeta_2\omega_2\mu\dot{z}_2 - \omega_2^2\mu z_2 = (F_0/m_1)e^{i\omega t}, \tag{3.3}$$

$$\ddot{z}_2 + 2\zeta_2\omega_2(1+\mu)\dot{z}_2 + \omega_2^2(1+\mu)z_2 - 2\zeta_1\omega_1\dot{z}_1 - \omega_1^2 z_1 = -(F_0/m_1)e^{i\omega t}, \tag{3.4}$$

or in matrix form suitable for numerical solution, writing $\xi_1 = \dot{z}_1, \xi_2 = \dot{z}_2$,

$$\begin{pmatrix} \dot{\xi}_1 \\ \dot{z}_1 \\ \dot{\xi}_2 \\ \dot{z}_2 \end{pmatrix} = \begin{pmatrix} -2\zeta_1\omega_1 & -\omega_1^2 & 2\zeta_2\omega_2\mu & \omega_2^2\mu \\ 1 & 0 & 0 & 0 \\ 2\zeta_1\omega_1 & \omega_1^2 & -2\zeta_2\omega_2(1+\mu) & -\omega_2^2(1+\mu) \\ 0 & 0 & 1 & 0 \end{pmatrix} \begin{pmatrix} \xi_1 \\ z_1 \\ \xi_2 \\ z_2 \end{pmatrix} + \begin{pmatrix} (F_0/m_1)e^{\omega t} \\ 0 \\ -(F_0/m_1)e^{\omega t} \\ 0 \end{pmatrix}. \tag{3.5}$$

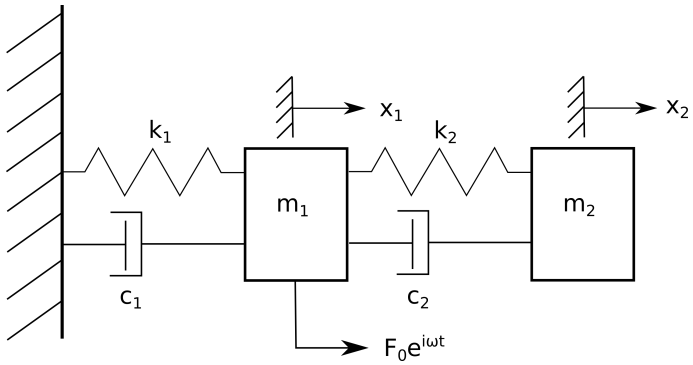

Figure 3.1 2DOF system with a harmonic force applied to mass m_1.

3.2 The free undamped 2DOF system, initial value problem

Equations 3.1 and 3.2 with $F_0 = 0$ and $\zeta_1 = \zeta_2 = 0$ read

$$\ddot{z}_1 + \omega_1^2 z_1 - \omega_2^2 \mu z_2 = 0, \tag{3.6}$$

$$\ddot{z}_2 + \omega_2^2(1+\mu) z_2 - \omega_1^2 z_1 = 0. \tag{3.7}$$

These equations have solutions on the form $\tilde{Z}e^{\omega^* t}$. Substitution into (3.6 and 3.7) gives the characteristic equation

$$\begin{pmatrix} (-\omega^{*2} + \omega_1^2) & -\omega_2^2\mu \\ -\omega_1^2 & (-\omega^{*2} + \omega_2^2(1+\mu)) \end{pmatrix} \begin{pmatrix} \tilde{Z}_1 \\ \tilde{Z}_2 \end{pmatrix} = \begin{pmatrix} 0 \\ 0 \end{pmatrix}. \tag{3.8}$$

which gives the following equation for the eigen-frequencies ω^*

$$\omega^{*4} - \left\{\omega_1^2 + \omega_2^2(1+\mu)\right\} \omega^{*2} + \omega_1^2\omega_2^2 = 0. \tag{3.9}$$

Let $\alpha = (\omega_2/\omega_1)^2$, then $\alpha\mu = k_2/k_1$ and the roots of (3.9) become

$$2(\omega^*/\omega_1)^2 = 1 + (1+\mu)\alpha \pm \sqrt{(1-\alpha)^2 + (2 + 2\alpha + \mu\alpha)\mu\alpha}. \tag{3.10}$$

For $\alpha \geq 0$ and $\mu \geq 0$, the discriminant is positive or zero. The natural frequencies of the system are ω_1 and ω_2 and the eigen frequencies are ω_1^* and ω_2^* given by expression (3.10).

It can be shown after sorting $\omega_1 < \omega_2$, that $(\omega_{1,2}^*/\omega_1)^2 \geq 0$ and that $\omega_1^* < \omega_1$, see appendix D. We have $\omega_1^{*2}\omega_2^{*2} = \omega_1^2\omega_2^2$ which implies that $\omega_2 < \omega_2^*$. Adding the two solutions of (3.10) gives

$\omega_1^{*2} + \omega_2^{*2} = \omega_1^2 + (1+\mu)\omega_2^2$, showing by itself that the separation between the eigen frequencies is larger than the separation between the natural frequencies. We summarize $\omega_1^* < \omega_1 < \omega_2 < \omega_2^*$. This behavior is demonstrated in a case treated below, see also figure 3.11

We can write the eigenvectors as

$$L_{1,2} = \begin{pmatrix} 1 \\ (-\omega_{1,2}^{*2} + \omega_1^2)/\mu\omega_2^2 \end{pmatrix}. \tag{3.11}$$

Since $\omega_1^* < \omega_1 < \omega_2 < \omega_2^*$, the second component of the first eigenvector L_1 is positive, while the second component of the second eigenvector L_2 is negative. In the first case m_1 an m_2 move in the same direction while in the second case they move oppositely.
As example, consider the case $k_1 = k_2 = k$. Then $\alpha = 1/\mu$ and from equation (3.10) we get the eigen frequencies

$$\omega_1^{*2} = \left(1 + \frac{1}{2\mu} - \sqrt{1 + \frac{1}{4\mu^2}}\right)\omega_1^2, \quad \omega_2^{*2} = \left(1 + \frac{1}{2\mu} + \sqrt{1 + \frac{1}{4\mu^2}}\right)\omega_1^2, \tag{3.12}$$

implying that $\omega_1^{*2} + \omega_2^{*2} = (2 + 1/\mu)\omega_1^2$.

Substitution of the solutions $z_1 = \tilde{Z}_1 e^{\omega_1^* t}$ and $z_2 = \tilde{Z}_2 e^{\omega_2^* t}$ into (3.8) gives the eigenvectors

$$L_1 = \begin{pmatrix} 1 \\ -\frac{1}{2\mu}\left(1 - \sqrt{4\mu^2 + 1}\right) \end{pmatrix}, \tag{3.13}$$

$$L_2 = \begin{pmatrix} 1 \\ -\frac{1}{2\mu}\left(1 + \sqrt{4\mu^2 + 1}\right) \end{pmatrix}. \tag{3.14}$$

The solution of the coupled 2DOF system is written as a sum of the *normal modes*

$$\begin{pmatrix} z_1 \\ z_2 \end{pmatrix} = \tilde{Z}_1 L_1 \sin(\omega_1^* t + \psi_1) + \tilde{Z}_2 L_2 \sin(\omega_2^* t + \psi_2).$$

The amplitudes $\tilde{Z}_1$ and $\tilde{Z}_2$ and phases ψ_1 and ψ_2 depend on the initial conditions. As an example, let $\mu = 1/2, m_1 = m, m_2 = m/2$ then $\omega_1 = \sqrt{k/m}$, and with initial conditions

$$\begin{pmatrix} z_1 \\ z_2 \end{pmatrix} = \begin{pmatrix} x_0 \\ 0 \end{pmatrix} \quad \text{and} \quad \begin{pmatrix} \dot{z}_1 \\ \dot{z}_2 \end{pmatrix} = \begin{pmatrix} 0 \\ 0 \end{pmatrix},$$

the solution can explicitly be written

$$\begin{aligned} z_1/x_0 =& \frac{1}{2}\left(1 + \frac{1}{\sqrt{2}}\right)\cos\left\{\left(\sqrt{(2-\sqrt{2})}\right)\omega_1 t\right\} + \frac{1}{2}\left(1 - \frac{1}{\sqrt{2}}\right)\cos\left\{\left(\sqrt{(2+\sqrt{2})}\right)\omega_1 t\right\}, \\ z_2/x_0 =& \frac{1}{2\sqrt{2}}\cos\left\{\left(\sqrt{(2-\sqrt{2})}\right)\omega_1 t\right\} - \frac{1}{2\sqrt{2}}\cos\left\{\left(\sqrt{(2+\sqrt{2})}\right)\omega_1 t\right\}. \end{aligned}$$

A plot of the solution is shown in figure 3.2. Notice that the solution is non-periodic.

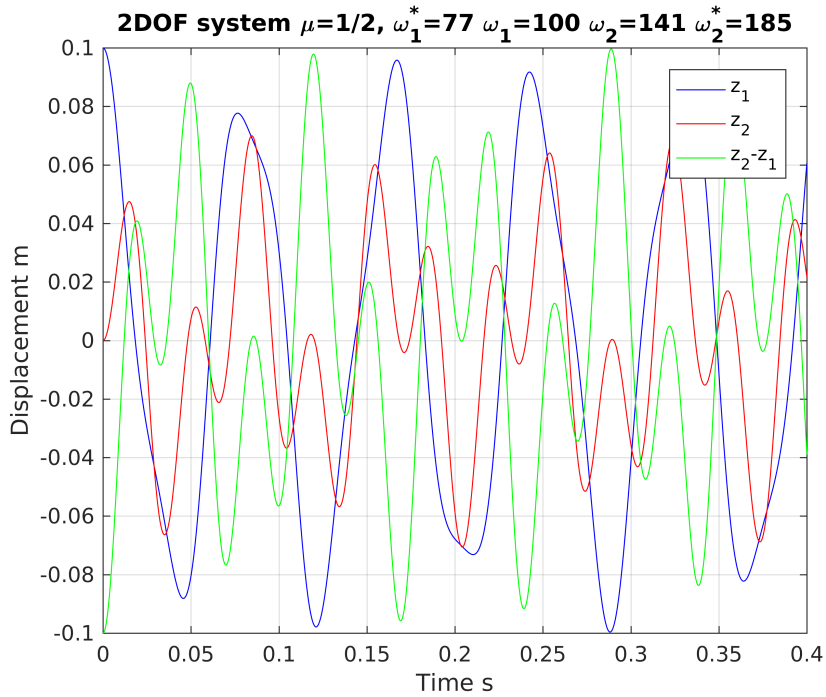

Figure 3.2 Displacement in a 2DOF system without damping. Initial conditions are $(z_1, z_2) = (0.1, 0), (\dot{z}_1, \dot{z}_2) = (0, 0)$.

3.3 Forced undamped 2DOF systems, resonances

Consider the system defined by equation 3.5 with $\zeta_1 = \zeta_2 = 0$. The response of the 2DOF system to the forcing $F_0 e^{i\omega t}$ is on the form $z_{1,2} = \tilde{Z}_{1,2} e^{i\omega t}$. Substitution of the solution into equation 3.5 gives the algebraic equation

$$\begin{pmatrix} -\omega^2 + \omega_1^2 & -\omega_2^2 \mu \\ -\omega_1^2 & -\omega^2 + \omega_2^2(1+\mu) \end{pmatrix} \begin{pmatrix} \tilde{Z}_1 \\ \tilde{Z}_2 \end{pmatrix} = \begin{pmatrix} F_0/m_1 \\ -F_0/m_1 \end{pmatrix}. \tag{3.15}$$

Solving this equation gives the amplitudes

$$\begin{aligned} \tilde{Z}_1 = \tilde{X}_1 &= \frac{F_0}{m_1} \cdot \frac{-\omega^2 + \omega_2^2}{\omega^4 - \left\{\omega_1^2 + \omega_2^2(1+\mu)\right\} \omega^2 + \omega_1^2 \omega_2^2}, \\ \tilde{Z}_2 &= \frac{F_0}{m_1} \cdot \frac{\omega^2}{\omega^4 - \left\{\omega_1^2 + \omega_2^2(1+\mu)\right\} \omega^2 + \omega_1^2 \omega_2^2}, \\ \tilde{X}_2 &= \frac{F_0}{m_1} \cdot \frac{\omega_2^2}{\omega^4 - \left\{\omega_1^2 + \omega_2^2(1+\mu)\right\} \omega^2 + \omega_1^2 \omega_2^2}. \end{aligned}$$

The case $k = k_1 = k_2$, $\mu = 1/2$ gives

$$\frac{\tilde{X}_1 k_1}{F_0} = \frac{\tilde{Z}_1 k_1}{F_0} = \frac{2 - (\omega/\omega_1)^2}{(\omega/\omega_1)^4 - 4(\omega/\omega_1)^2 + 2}, \tag{3.16}$$

$$\frac{\tilde{Z}_2 k_1}{F_0} = \frac{(\omega/\omega_1)^2}{(\omega/\omega_1)^4 - 4(\omega/\omega_1)^2 + 2}, \tag{3.17}$$

$$\frac{\tilde{X}_2 k_1}{F_0} = \frac{2}{(\omega/\omega_1)^4 - 4(\omega/\omega_1)^2 + 2}. \tag{3.18}$$

When the denominator $(\omega/\omega_1)^4 - 4(\omega/\omega_1)^2 + 2 = 0$, resonances occur, which is at the eigen frequencies ω_1^* an ω_2^*. Figure 3.3 shows a plot of the normalized amplitudes, the resonances and at $\omega = \sqrt{2}\omega_1 = \omega_2$, $X_1 = 0$, by setting the nominator of (3.16) to zero, where the Frahm/dynamic damping occurs, see also discussion in appendix B.

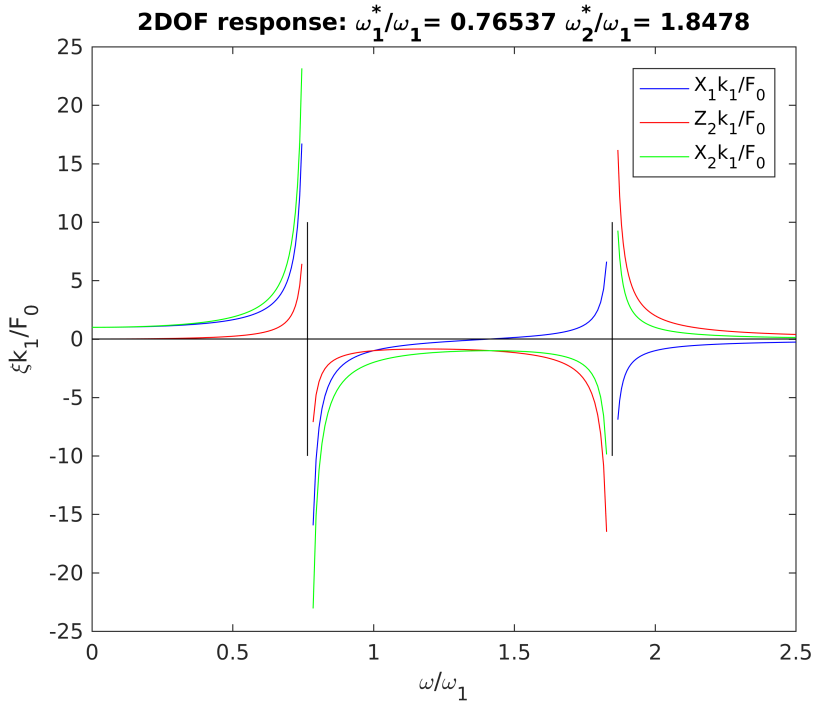

Figure 3.3 Forced response of the 2DOF system described by formulas (3.16),(3.17),(3.18). The blue curve crosses 0 *at* $\omega = \sqrt{2}\omega_1 = \omega_2$*, which is where* m_2 *absorbs maximum energy and the motion of* m_1 *is optimally damped. The vertical black lines at* $\omega/\omega_1 = 0.76537, 1.9478$ *expresses the eigen frequencies* ω_1^* *and* ω_2^* *which defines the normal modes.*

3.4 Numerical solutions of the forced 2DOF system. Harmonic excitation.

We consider three cases: First, the dynamic vibration absorber, $f_{ex} = f_2$. Second, excitation at first resonance $f_{ex} = f_1^*$. Third, excitation at second resonance $f_{ex} = f_2^*$. The oscillations start with initial conditions $z_1 = z_2 = 0, \dot{z}_1 = \dot{z} = 0$ and with a force $F(t) = 0$, for $t < 0$, and $F(t) = F_0 \sin \omega t$, for $t \geq 0$. We use RK45 for the numerical solution of equation 3.19 written as a first order system. Let $\xi_i = \dot{z}_i, i = 1, 2$, then

$$\begin{pmatrix} \dot{\xi}_1 \\ \dot{z}_1 \\ \dot{\xi}_2 \\ \dot{z}_2 \end{pmatrix} = \begin{pmatrix} -2\zeta_1\omega_1 & -\omega_1^2 & 2\zeta_2\omega_2\mu & \omega_2^2\mu \\ 1 & 0 & 0 & 0 \\ 2\zeta_1\omega_1 & \omega_1^2 & -2\zeta_2\omega_2(1+\mu) & -\omega_2^2(1+\mu) \\ 0 & 0 & 1 & 0 \end{pmatrix} \begin{pmatrix} \xi_1 \\ z_1 \\ \xi_2 \\ z_2 \end{pmatrix} + \begin{pmatrix} (F_0/m_1)\sin\omega t \\ 0 \\ -(F_0/m_1)\sin\omega t \\ 0 \end{pmatrix}. \tag{3.19}$$

The accelerations become as follows

$$\begin{aligned} \ddot{x}_1 &= -2\zeta_1\omega_1\xi_1 - \omega_1^2 z_1 + 2\zeta_2\omega_2\mu\xi_2 + \omega_2^2\mu z_2 + (F_0/m_1)\sin\omega t, \\ \ddot{x}_2 &= -2\zeta_2\omega_2\xi_1 - \omega_2^2 z_2. \end{aligned}$$

The solutions shows transient behavior from zero oscillation through a transient phase to a quasi equilibrium phase with nearly harmonic oscillations.

The results are shown in figures 3.4, 3.5 and 3.6. For the dynamic damper, the transient solution reaches an equilibrium state close to zero amplitude for mass m_1. The energy is taken up by oscillator m_2 which reaches equilibrium where the dissipated energy equals energy added by the harmonic force. This happen although the harmonic force acts at m_1, that mass reaches hardly any motion. The result is shown in figure 3.4.

If the system is forced at the eigen-frequency $f_{ex} = f_1^*$, or $f_{ex} = f_2^*$, equilibrium states are reached where the energy input from the force is balanced by viscous dissipation. The results are shown in figure 3.5 and 3.6. Notice the difference of figure 3.4 and 3.6. The difference in frequency $f_2 = 20\,Hz$ and $f_2^* = 21.2\,\text{Hz}$ is small, indicating that the Frahm damper works for oscillations in a limited frequency band.

The amplitude $\tilde{X}_2 = -F_0/k_2$ is derived in appendix B. With input $F_0 = 10\,\text{N}$, period $\tau_2 = 0.05\,\text{s}$, mass fraction $\mu = m_2/m_1 = 0.1$, we get $\tilde{X}_2 = 0.0063\,\text{m}$, to which the solution approaches, see figure 3.4.

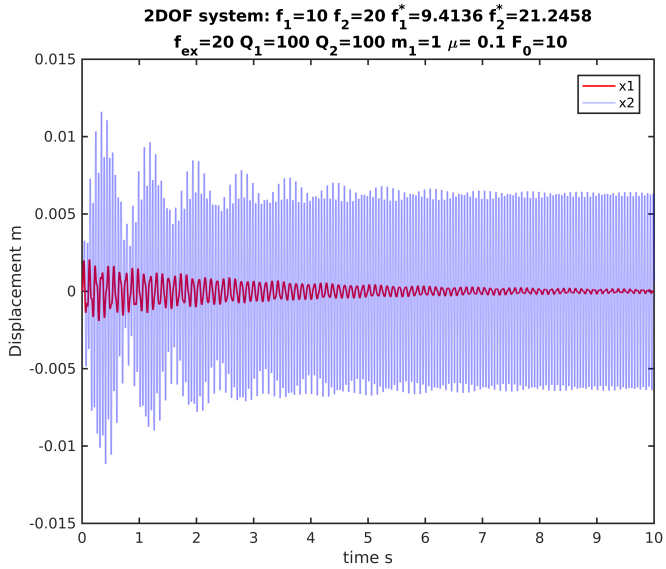

Figure 3.4 *Forced 2DOF system, dynamic vibration damper. The displacements x_1 and x_2 are shown. In this case the eigen-frequencies of the system are $f_1^* = 9.4\,Hz$ and $f_2^* = 21.2\,Hz$. The natural frequencies $f_{1,2} = (1/2\pi)\sqrt{k_{1,2}/m_{1,2}} = 10, 20\,Hz$. $\mu = 0.1$. The excitation frequency $f_{ex} = f_2 = 20\,Hz$. Quality factors $Q_1 = Q_2 = 100$ and forcing amplitude is $F_0 = 10\,N$. The displacement of m_1 approaches zero.*

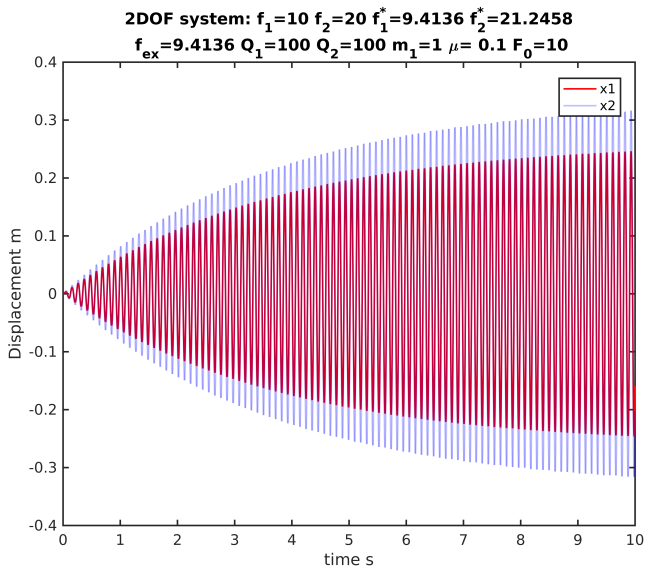

Figure 3.5 *Forced 2DOF system. The displacements x_1 and x_2 are shown. The eigen-frequencies are $f_1^* = 9.4\,Hz$ and $f_2^* = 21.3\,Hz$, the natural frequencies are $f_{1,2} = (1/2\pi)\sqrt{k_{1,2}/m_{1,2}} = 10, 20\,Hz$, $\mu = 0.1$ and the excitation frequency equals the eigen-freqeuency $f_{ex} = f_1^*$. Quality factors are $Q_1 = Q_2 = 100$ and forcing amplitude is $F_0 = 10\,N$. The displacements approaches some finite amplitude.*

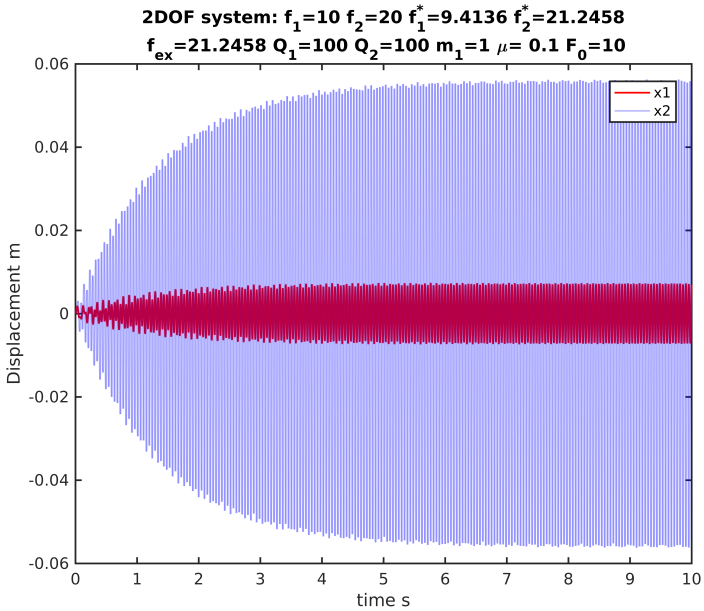

Figure 3.6 Forced 2DOF system. Same as figure 3.5 except that $f_{ex} = f_2^*$.

3.5 Support motion on 2DOF systems

Consider a damped 2DOF system excited by a moving base/support. The system is shown in figure 3.7 and described by the equations 3.20 and 3.21.

$$m_1\ddot{x}_1 = -k_1(x_1 - y) - c_1(\dot{x}_1 - \dot{y}) + k_2(x_2 - x_1) + c_2(\dot{x}_2 - \dot{x}_1), \tag{3.20}$$

$$m_2\ddot{x}_2 = -k_2(x_2 - x_1) - c_2(\dot{x}_2 - \dot{x}_1). \tag{3.21}$$

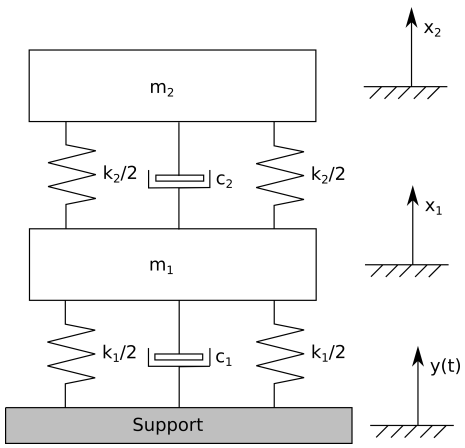

Figure 3.7 Support motion, 2DOF system.

Most authors use the substitutions $z_1 = x_1 - y, z_2 = x_2 - y$, etc. . .
Instead we use the substitution $z_1 = x_1 - y,\ z_2 = x_2 - x_1,\ \mu = m_2/m_1$ which gives nice symmetry of the governing equations. Substitution into equations (3.20) and (3.21) gives

$$m_1\ddot{x}_1 = -k_1 z_1 - c_1\dot{z}_1 + k_2 z_2 + c_2\dot{z}_2, \tag{3.22}$$

$$m_2\ddot{x}_2 = -k_2 z_2 - c_2\dot{z}_2, \tag{3.23}$$

and

$$m_1\ddot{z}_1 + c_1\dot{z}_1 + k_1 z_1 = -m_1\ddot{y} + c_2\dot{z}_2 + k_2 z_2, \tag{3.24}$$

$$m_2\ddot{z}_2 + c_2\dot{z}_2 + k_2 z_2 = -m_2\ddot{x}_1. \tag{3.25}$$

Notice the symmetry of these equations. Particularly the motion of m_1 acts in the same way on m_2 as the motion of the support $\ddot{y}$ does on m_1, but with some corrections on m_1 through the motion of m_2. The viscous and spring forces from m_2 on m_1 act through the terms $c_2\dot{z}_2 + k_2 z_2$. After substitution of $\ddot{x}_1$ from (3.22) into (3.25) we get the system

$$m_1\ddot{z}_1 + c_1\dot{z}_1 + k_1 z_1 - c_2\dot{z}_2 - k_2 z_2 = -m_1\ddot{y}, \tag{3.26}$$

$$m_2\ddot{z}_2 + c_2(1+\mu)\dot{z}_2 + k_2(1+\mu)z_2 - \mu_1 c_1\dot{z}_1 - \mu k_1 z_1 = 0. \tag{3.27}$$

Now with $2\zeta_i\omega_i = c_i/m_i,\ \omega_i^2 = k_i/m_i,\ i = 1, 2$ we finally have

$$\ddot{z}_1 + 2\zeta_1\omega_1\dot{z}_1 + \omega_1^2 z_1 - 2\zeta_2\omega_2\mu\dot{z}_2 - \omega_2^2\mu z_2 = -\ddot{y}, \tag{3.28}$$

$$\ddot{z}_2 + 2\zeta_2\omega_2(1+\mu)\dot{z}_2 + \omega_2^2(1+\mu)z_2 - 2\zeta_1\omega_1\dot{z}_1 - \omega_1^2 z_1 = 0. \tag{3.29}$$

Solving these equations give z and $\dot{z}$ and we can calculate the accelerations as

$$\ddot{x}_1 = -2\zeta_1\omega_1\xi_1 - \omega_1^2 z_1 + 2\zeta_2\omega_2\mu\xi_2 + \omega_2^2\mu z_2, \tag{3.30}$$

$$\ddot{x}_2 = -2\zeta_2\omega_2\xi_2 - \omega_2^2 z_2. \tag{3.31}$$

It is not difficult to extend the above derivation to the nDOF system, see details in appendix C.

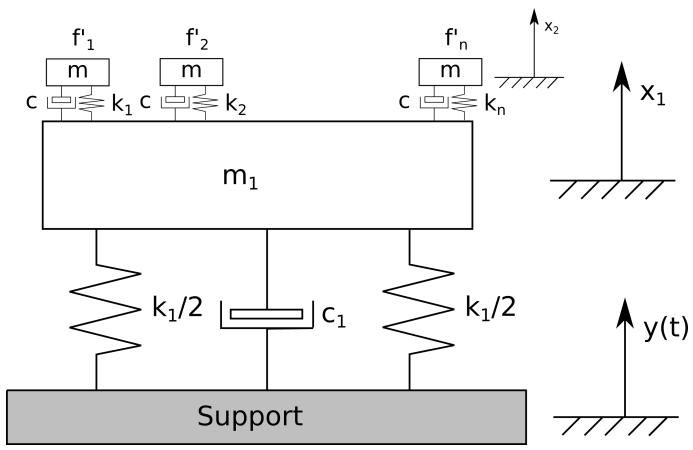

Figure 3.8 Shock response probes of 1DOF oscillators $f_1', f_2', \ldots, f_n'$ used to calculate SRS of an oscillator excited by a moving support. The shock response probe masses are small $\mu = m/m_1 << 1$ which implies no impact on the motion of m_1.

We can calculate the SRS of an oscillator m_1 excited by a support motion system in two ways:
1) Using a sDOF base motion system to calculate the oscillation of m_1 i.e $\ddot{x}_1$ as input as base motion for a sDOF for m_1. See figure 3.8.
2) Using a 2DOF base excited system with $m_2 << m_1$ to calculate the oscillation of m_1 and m_2 and using the set of oscillators m_2 as SRS probes for m_1.

A 2DOF base excited system is used to calculate motions of both m_1 and m_2 for any masses. The motion of the two masses is coupled. The accelerations $\ddot{x}_1$ and $\ddot{x}_2$ can be written to files or memory and both be used as base motion for shock response spectra for both m_1 and m_2.

An example of shock response spectra of a set of sDOF oscillators excited by double half-sine base motion is shown in figure 3.10. The black curve shows the SRS of the base motion. The colored curves shows Shock Response Spectra of the various sDOF oscillators. For all oscillators, there is a maximum in the SRS at their natural frequency. In the low frequency regime, the spectra approach the base SRS.

Figure 3.9 shows the SRS of double half-sine base motion as a black curve. We use a SRS probes to calculate the SRS of the base and we use a second set of probes to calculate the SRS of the "probe of the base". The SRS of an oscillator of natural frequency $f_1 = 39.7$ Hz is shown as the blue curve. This oscillator is the SRS probe for the base generating the point where on the base

SRS where the red vertical line $f_1 = 39.6825$ Hz and the black curve crosses. The blue curve is the SRS of the SRS probe for the base motion. At high frequencies the blue curve approaches the maximum (maximax) acceleration of the base motion probe which is the red horizontal line. This is shown in figure 3.9.

Figure 3.10 shows the SRS of various oscillators with natural frequencies $f = 40, 79, 159, 317, 635$ Hz. All of them has asymptotic values at high frequencies that approach to the base SRS for which that particular oscillator has its natural frequency. The base SRS is shown as a black curve.

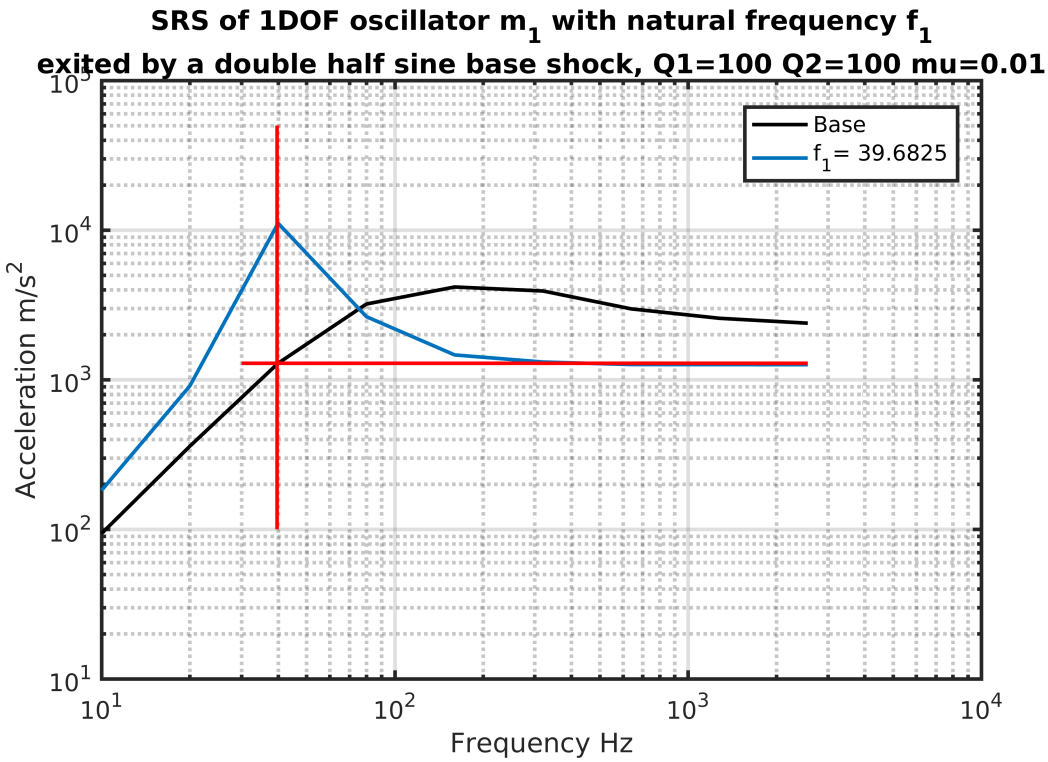

Figure 3.9 *The black curve shows SRS of base motion, which is a double half-sine shock. The blue curve shows the SRS of an sDOF oscillator m_1 with natural frequency $f_1 = 39.68$ Hz, excited by base motion, see figure 3.8. At the same time, oscillator m_1 which natural frequency is f_1 is one of the SRS probes of the base. It has maximax at f_1 indicated by the red horizontal line at $1260\,m/s^2$. The SRS of m_1 will asymptotically approach that value which is shown in the figure. The reason for the relatively high max value of the blue curve is due to the oscillatory motion of m_1.*

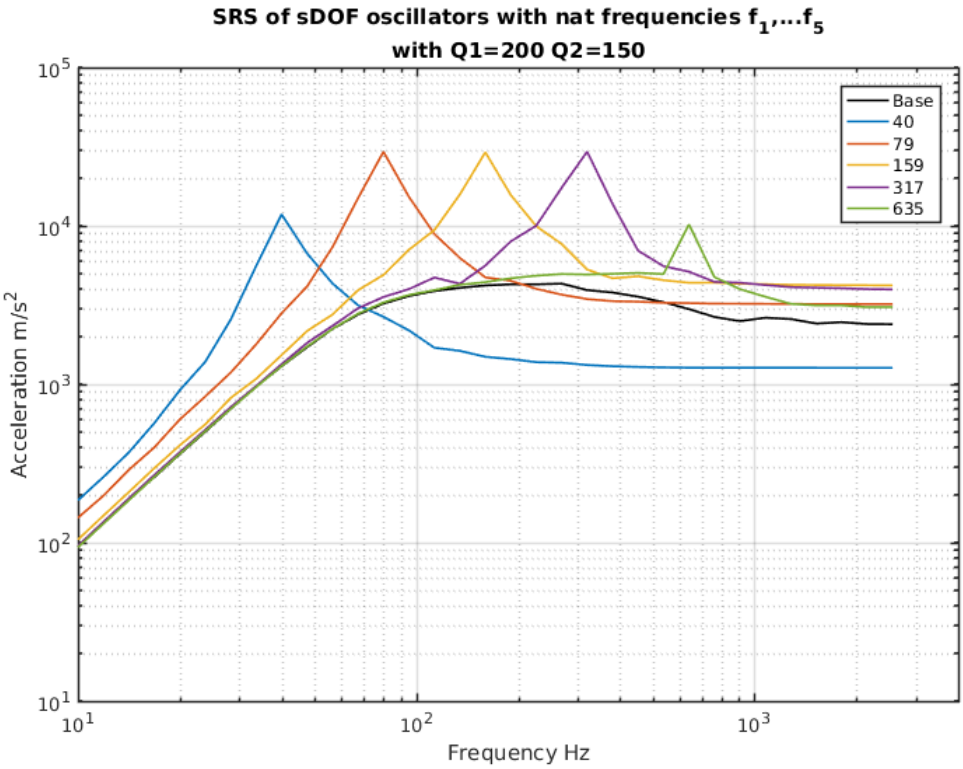

Figure 3.10 *Shock response spectra of sDOF oscillators with various natural frequencies f_i showed by the colored curves. The oscillators are excited by the double half-sine base shock as defined in figure 2.4. In this case the SRS of the sDOF systems are calculated as a 2DOF system where the mass fraction $\mu = m_2/m_1 = 0.01$, so the probe masses m_2 has no impact on the motion of m_1. The SRS of the base motion is shown by the black curve. The frequencies of the oscillators are* $40, 79, 159, 317, 635$ *Hz.*

3.6 The shock spectrum dip effect

Shock spectrum dips may occur in nDOF system and we will use the 2DOF system to demonstrate the effect. The shock spectrum dip was demonstrated experimentally by O'Hara [14] and later explained by a mathematical model in [15]. The shock spectrum dip effect is important when making Shock Design Spectra. As we can see in figure 3.11 there are two strong maxima with a dip in between. What value should be considered as design criteria for equipment mounted for example to a ship structure? O'Hara has shown that when taking into consideration the peaks of the spectrum, unrealistic over-design will occur and that the better more realistic design values are rather the minimum accelerations found in the dip. This is of course very important when it comes to design of ship structures.

For a 2DOF system we have shown that the spectral distance between the eigen frequencies are wider than the distance between the natural frequencies. In addition, the lowest eigen frequency $\omega_1^* < \omega_1$ is lower than the lowest natural frequency and the highest eigen frequency if higher than the highest natural frequency, $\omega_2 < \omega_2^*$. The double half-sine shock is broad banded, exciting the masses m_1 and m_2 in a wide frequency band. The SRS of the system contains two local maxima, one at each eigen frequency. Between them is a minimum which is located at ω_2 and close to ω_1. The reason for this minimum is that m_2 acts as a dynamic vibration absorber removing energy around $\omega = \omega_2$.

Consider the 2DOF system shown in figure 3.7. Let the acceleration of the support be according to the double half-sine described in figure 2.4. We solve the equations numerically and construct the SRS from the solutions. We calculate the SRS from the motion of both mass m_1 and m_2 which is coupled. The result is shown in figure 3.11. The dip in the spectrum is evident. There is a dip for both masses. The natural frequencies are marked with vertical lines. Notice that the level of the SRS of m_1 at the frequency f_2 reaches the SRS of the base which is drawn by the black curve.

A tripartite SRS plot of the 2DOF system is shown in figure 3.12.

3.7 Shock response and the 3DOF system

The 3DOF SRS system is only briefly treated in this section. We consider a 3DOF support motion system excited by the double half-sine pulse defined in figure 2.4. The dynamic equations of the nDOF support motion system is summarized in appendix C. The 3DOF case is considered as an example in the same appendix. A particular case is presented here with $f_1 = 3.3$, $f_2 = 142.85$, $f_3 = 40\,\text{Hz}$ and $\mu_{21} = m_2/m_1 = 2$, $\mu_{32} = m_3/m_2 = 0.5$, the resulting SRS is shown in the figure 3.13. The SRS of m_1 has three local maxima and two dips. Notice also that the SRS of m_1 and m_3 are nearly similar while the SRS level of m_2 is nearly 5-times larger than the other two. We also notice that the SRS of the base motion is lower only in the low frequency part of the spectrum indicating that the shock response is lowered in the high frequency part of the spectrum (compared with the 2DOF system). We also see the same trend with shock response dips, in the 3DOF system, two dips.

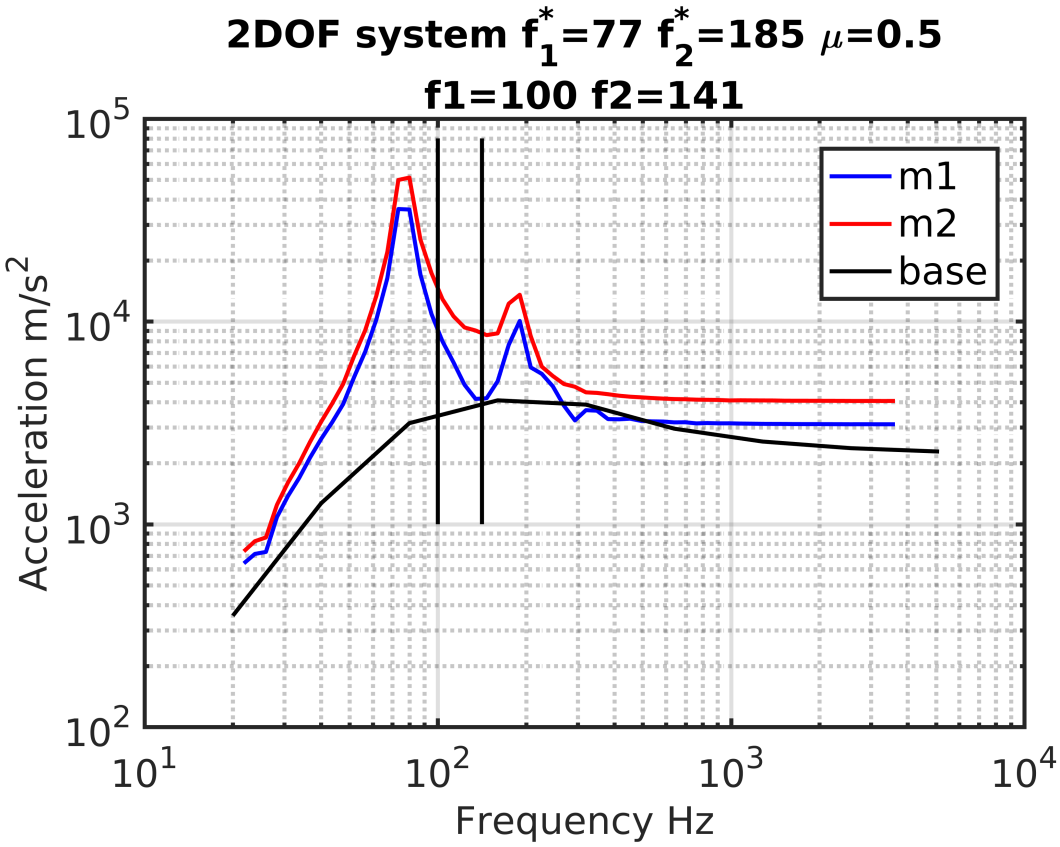

Figure 3.11 *SRS of 2DOF system shown in figure 3.7 excited by a double half-sine pulse defined in figure 2.4. Shock response spectra are calculated for m_1, blue curve, for m_2, red curve and the base, black curve. The red and blue curves have nearly the same form. The system has natural frequencies $f_1 = 100\,Hz$ and $f_2 = 141\,Hz$ marked by the vertical black lines. The eigen-frequencies are $f_1^* = 77\,Hz$ and $f_2^* = 185\,Hz$. Here we find local peaks in the spectra. The SRS is depressed at the natural frequencies. At f_2, the SRS of m_1 has a local minimum at the level of the SRS of the base. This minimum can be explained by the theory of the dynamic vibration absorber, see appendix B.*

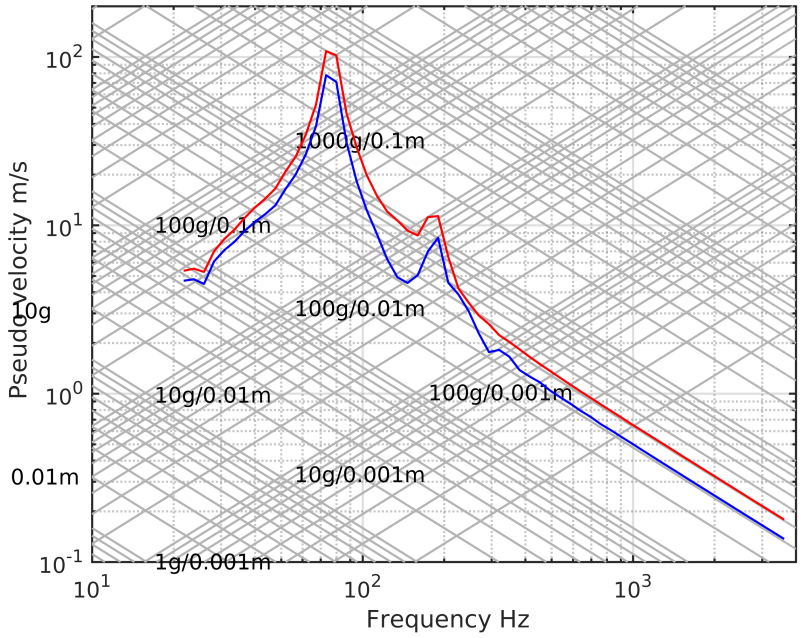

Figure 3.12 Tripartite plot of SRS of the same 2DOF system as shown in figure 3.11.

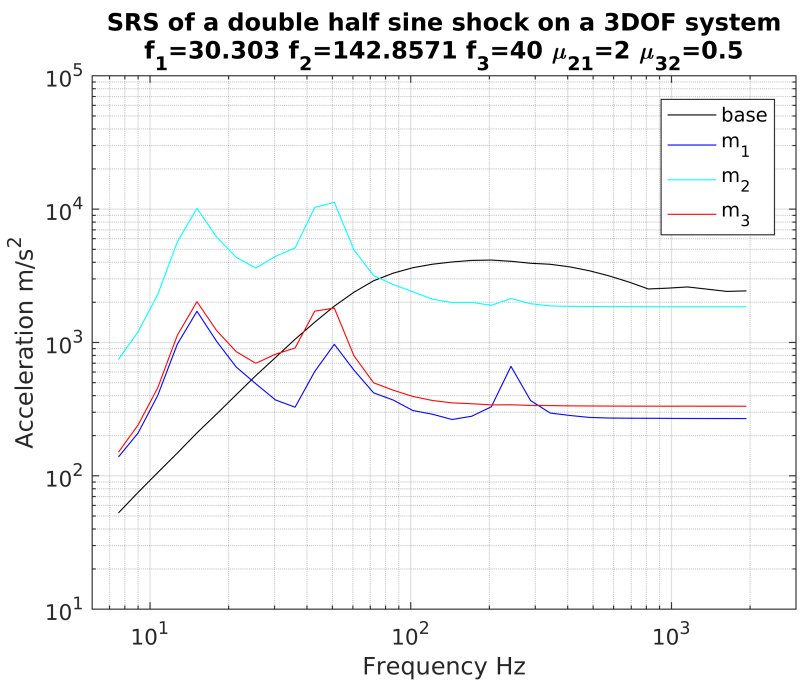

Figure 3.13 SRS of a 3DOF system with the double half-sine support pulse as defined in figure 2.4.

4 The double beam experiment

A scale model of the double beam system used by O'Hara [15] to demonstrate the shock response spectrum dip was tested in the shaker at FFI's Environment Lab. The drawing of the beam system is shown in figure 4.1. The double beam system is mechanically equivalent with a 2DOF system. The two eigen frequencies can be varied by changing masses and/or beam stiffness. We tested only a single configuration.

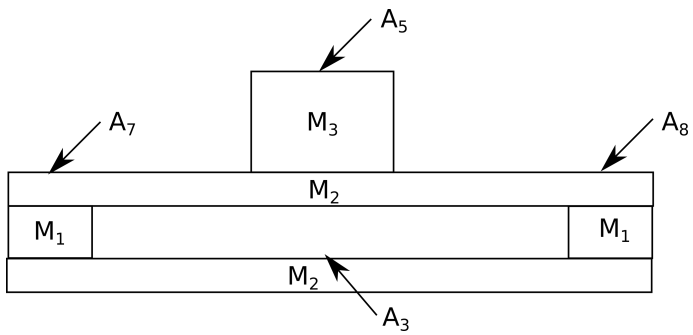

Figure 4.1 Sketch of the double beam system with the masses and accelerometer positions. The shaker attack at point A_3.

The double beam was attached to the shaker at a span wise oriented narrow beam at point A_3. To access the eigen frequencies, two control accelerometers were attached to the spanwise beam which was clamped to the head expanding plate of the shaker. The shaker was programmed to produce a white noise random signal. The output of the control accelerometers shows a flat spectrum. In figure 4.2, power spectral density plots of the signals obtained from accelerometers A_3, A_5 and A_7, (Accelerometers and channels are linked as follows $A_3 \leftrightarrow ch1$, $A_5 \leftrightarrow ch4$, $A_7 \leftrightarrow ch5$) during the random test are shown. Accelerometer A_3 is a control accelerometer while A_5 is at the mid top and A_7 is at the side. Maxima in response is shown and marked in figure 4.2. The lines at 100, 200 Hz and 300 Hz are artificial. We observe peaks in the spectrum at 23.8, 28.8 Hz and 63.8, 81.3 Hz.
A double half-sine pulse in acceleration was then generated by the shaker. A subset of the accelerations from A_3, A_5 and A_7 is shown in figure 4.3. The dark blue curve shows that the shaker gives a reasonable double half-sine pulse.

From figure 4.2 we see local maxima in the spectrum.

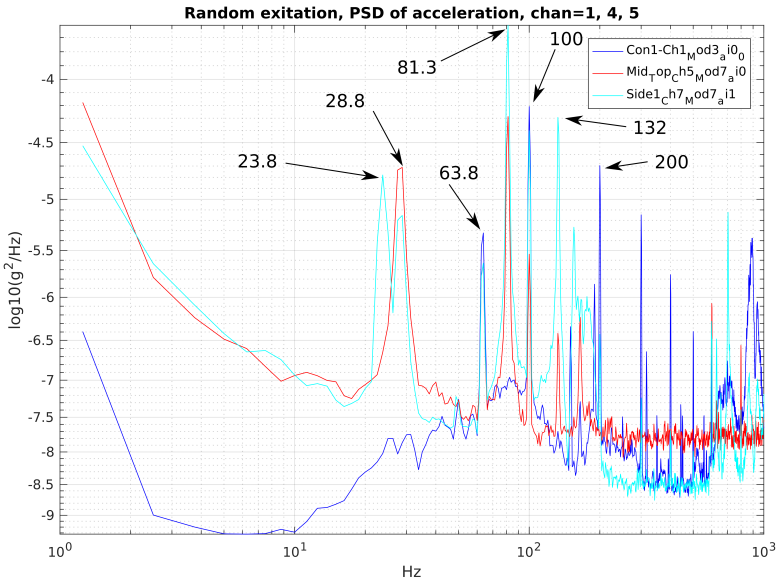

Figure 4.2 PSD of accelerometer 1, 5 and 7 from shaker test applying a random noise signal to reveal resonances. We observe that both center and side accelerometer signals have peaks at $f = 28$ and 81 Hz.

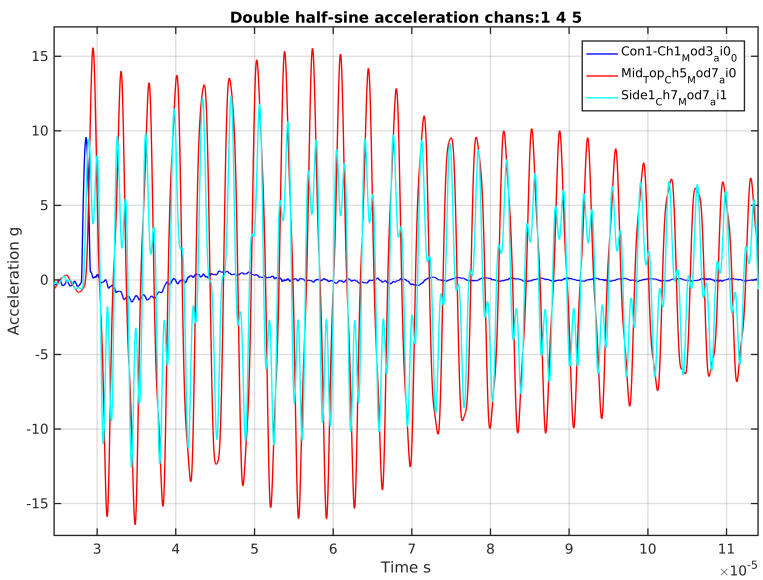

Figure 4.3 Double half-sine accelerations applied to beam by an electromagnetic shaker. The black curve represents base motion, red curve, mid acceleration and blue curve, side acceleration.

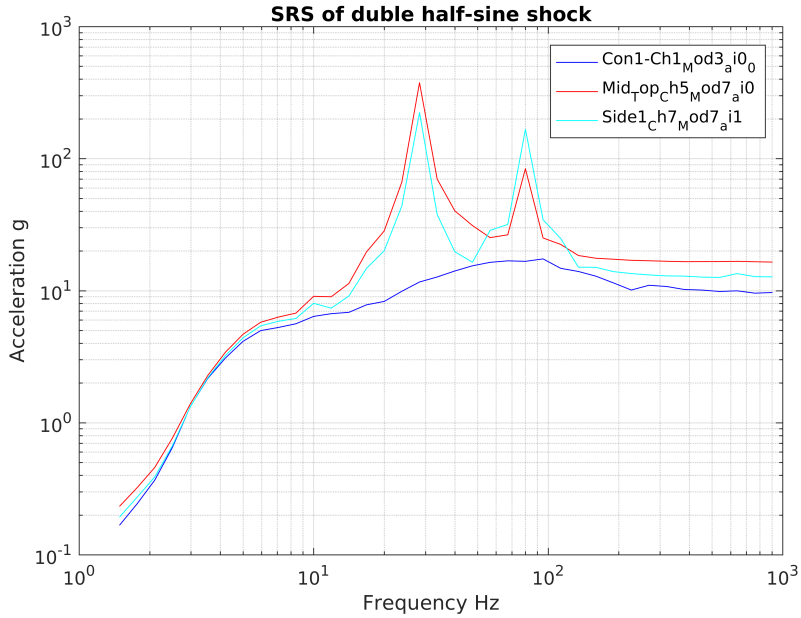

Figure 4.4 *The figure contains three curves showing SRS from accelerometer data from the double beam experiment. Black curve shows SRS of the base, red curve shows SRS of the mid while the blue curve shows the SRS of the side accelerometer. There are two strong peaks in the spectra representing the eigen frequencies of the system. They are at* 28 *and* 81 *Hz. Also the system resembles a 2DOF system and we notice the deep dip in the spectrum.*

5 Conclusion

The motivation for this report was to explain the physical meaning of the shock response spectrum using the sDOF supported motion model in a simple way containing detailed derivations and explanations.

Through the report, we have paid attention to the double half-sine shock pulse used by the German-Dutch navies as standard pulse for their shock classifications. Most examples are based on that pulse. We also explain how shock response spectra can be used as design criteria and how they are used in the characterization of shocks.

Tripartite plots are conveniently used to present shock response spectra. We explain what tripartite plots are and how to make them. Tripartite plots occur in design criteria specifying acceleration, velocity and displacement (a_0, v_0, d_0) in the plot which is equivalent for a double half-sine pulse to a specification of peak acceleration and time-spans for the double pulse (A, t_1, t_2). We have argued that a shock response spectrum can not be used to reproduce the acceleration of a shock. Compared with the Fourier transform of a dataset where the data can be retrieved from the transformed data, acceleration data can not be retrieved from its SRS. Anyway, the SRS offers sufficient accuracy in the design process.

The free 2DOF system, the 2DOF system with a harmonic force applied to m_1 and the 2DOF system excite by base motion are discussed as well as the dynamic vibration absorption. This is done to explain the *shock spectrum dip* effect which also is observed in physical experiments. Maxima in the SRS which occur in a 2DOF system will lead to an over specification in design. As a design criteria, it is better to use the dip in the 2DOF SRS system or the dips in the nDOF SRSs rather than local maxima. We have studied the SRS maxima of a 2DOF system and compared with the SRS maxima of the base excitation. The level in the dip of the SRS of the mass closest to the base m_1 has the same acceleration as the base. The dip occurs at the natural frequency of m_2 (comparable with the dynamic vibration absorption). The same effects are evident for the double beam which acts in analogy to a 2DOF spring system.

It is important to be aware that the effect *amplified repsonse* gives higher accelerations than the max peak acceleration of the base motion. This is due to resonant excitation.

There is not a unique relation between the acceleration pulse profile and the SRS. Several pulse profiles may give the same SRS. There seems to be a dispute that a given SRS is sufficient to imply a unique impact to an object irrespective of the acceleration profiles which may be different and at the same time cause the same SRS. The limitation of shakers in shock testing is discussed among experts. Some of them claim that a wanted SRS is sufficient for the test. This will extend the range were shakers can be used in shock testing.

A Analytical solution for the non-damped sDOF system

The equation for a SDOF system excited by a double half-sine pulse is

$$\ddot{z} + \omega_n^2 z = -\ddot{y} = -A_1 \begin{cases} \sin p_1 t, & 0 \le t \le t_1, \\ -\frac{t_1}{t_2 - t_1} \sin p_2 (t - t_1), & t_1 < t \le t_2, \\ 0, & t_2 < t, \end{cases} \tag{A.1}$$

where $p_1 = (\pi/t_1)$ and $p_2 = \pi/(t_2 - t_1)$, $R_1 = p_1/\omega_n$. For $0 \le t \le t_1$.

Equation (A.1) has solutions on the form

$$z(t) = A \sin \omega_n t + B \sin \omega_n t - \frac{A_1/\omega_n^2}{1 - (p_1/\omega_n)^2} \sin p_1 t. \tag{A.2}$$

Let $z(0) = 0, \dot{z}(0) = 0$ and write $K_1 = 1/(1 - (p_1/\omega_n)^2)$, we get

$$B = 0, \quad A = A_1 K_1 R_1 \frac{1}{\omega_n^2}, \quad \text{and we get for}$$

$$0 \le t \le t_1, \quad z(t) = A_1 \frac{K_1}{\omega_n^2} \Big(R_1 \sin \omega_n t - \sin p_1 t \Big).$$

From $x = z + y$, with $y = \frac{A_1}{p_1}(t - \frac{1}{p_1} \sin p_1 t)$, we get

$$x(t) = A_1 \frac{t}{p_1} + A_1 R_1 \frac{K_1}{\omega_n^2} \Big(\sin \omega_n t - R_1 \sin p_1 t \Big). \tag{A.3}$$

Undamped oscillator for $t_1 < t \le t_2$ we write

$$q = t_1/(t_2 - t_1), \quad p_2 = \pi/(t_2 - t_1),$$
$$R_2 = p_2/\omega_n, \quad K_2 = 1/(1 - (p_2/\omega_n)^2),$$

and $t' = t - t_1$, the solution is on the form

$$z_2(t) = A \sin \omega_n t' + B \cos \omega_n t' + A_1 K_2 (q/\omega_n^2) \sin p_2 t'. \tag{A.4}$$

We require that $z(t)$ and $\dot{z}(t)$ are both continuous at $t = t_1$

$$z_1(t_1) = z_2(t_1), \quad \Rightarrow$$

$$z_1(t_1) = A_1 K_1 (R_1/\omega_n^2) \sin \omega_n t_1 = B,$$

$$\dot{z}_1(t_1) = A_1 K_1 (R_1/\omega_n)(\cos \omega_n t_1 + 1),$$

$$\dot{z}_2(t_1) = A\omega_n + A_1 K_2 q (R_2/\omega_n),$$

$$\dot{z}_1(t_1) = \dot{z}_2(t_2),$$

$$\Downarrow$$

$$A = \frac{A_1}{\omega_n^2}(K_1 R_1 - K_2 R_2 q) + A_1 K_1 (R_1/\omega_n^2) \cos \omega_n t_1,$$

and we had

$$B = A_1 K_1 (R_1/\omega_n^2) \sin \omega_n t_1,$$

giving for $t_1 < t \leq t_2$

$$\begin{aligned} z_2(t) = \quad & (A_1/\omega_n^2)\left\{(K_1R_1 - K_2R_2q)\sin\omega_n(t-t_1)+\right. \\ & \left. K_1R_1\sin\omega_n t + K_2q\sin p_2(t-t_1)\right\}. \end{aligned} \tag{A.5}$$

For $t_2 < t$ the solution is on the form

$$z_3(t) = A\sin\omega_n(t-t_2) + B\cos\omega_n(t-t_2).$$

It is required that z and $\dot{z}$ are continuous, which gives

$$\begin{aligned} A = \quad & (A_1/\omega_n^2)\left\{(K_1R_1 - K_2R_2q)\cos\omega_n(t_2-t_1)+\right. \\ & \left. K_1R_1\cos\omega_n t_2 - K_2R_2q\right\}, \end{aligned} \tag{A.6}$$

$$\begin{aligned} B = \quad & (A_1/\omega_n^2)\left\{(K_1R_1 - K_2R_2q)\sin\omega_n(t_2-t_1)+\right. \\ & \left. K_1R_1\sin\omega_n t_2\right\}. \end{aligned} \tag{A.7}$$

Finally the solution with derived $\dot{z}, \ddot{z}, \ddot{x}$ can be written

$$\begin{aligned}
z_1(t) = \quad & (A_1/\omega_n^2)K_1\left\{R_1\sin\omega_n t - \sin p_1 t\right\}, \\
z_2(t) = \quad & (A_1/\omega_n^2)\left\{(K_1R_1 - K_2R_2q)\sin\omega_n(t-t_1)+\right. \\
& \left. K_1R_1\sin\omega_n t + K_2q\sin p_2(t-t_1)\right\}, \\
z_3(t) = \quad & A\sin\omega_n(t-t_2) + B\cos\omega_n(t-t_2), \\
\\
\dot{z}_1(t) = \quad & (A_1/\omega_n)K_1R_1\left\{\cos\omega_n t - \cos p_1 t\right\}, \\
\dot{z}_2(t) = \quad & (A_1/\omega_n)\left\{(K_1R_1 - K_2R_2q)\cos\omega_n(t-t_1)+\right. \\
& \left. K_1R_1\cos\omega_n t + K_2R_2q\cos p_2(t-t_1)\right\}, \\
\dot{z}_3(t) = \quad & A\omega_n\cos\omega_n(t-t_2) - B\omega_n\sin\omega_n(t-t_2), \\
\\
\ddot{z}_1(t) = \quad & -\omega_n^2 z_1(t) - A_1\sin p_1 t, \\
\ddot{z}_2(t) = \quad & -\omega_n^2 z_2(t) + A_1 q\sin p_2(t-t_1), \\
\ddot{z}_3(t) = \quad & -\omega_n^2 z_3(t), \\
\\
\ddot{x}_1(t) = \quad & -\omega_n^2 z_1(t), \\
\ddot{x}_2(t) = \quad & -\omega_n^2 z_2(t), \\
\ddot{x}_3(t) = \quad & -\omega_n^2 z_3(t).
\end{aligned} \tag{A.8}$$

B The Frahm vibration absorber

We apply a force $F_0 e^{i\omega t}$ to the mass m_1, see figure 3.1. As shown in the figure, a mass m_2 is attached to m_1 through a spring. Absorption of energy from mass m_1 will occur when the mass m_2 has natural frequency equal to the forcing frequency ω. This can be demonstrated as follows. Consider equations (3.3) and (3.4). Neglecting dissipation $\zeta_1 = \zeta_2 = 0$ and assuming $Z_1 = \tilde{Z}_1 e^{i\omega t}, Z_2 = \tilde{Z}_2 e^{i\omega t}$, then equations (3.3) and (3.4) implies

$$-\tilde{Z}_1\omega^2 + \tilde{Z}_1\omega_1^2 - \tilde{Z}_2\omega_2^2\mu = F_0/m_1, \tag{B.1}$$

$$-\tilde{Z}_2\omega^2 + \tilde{Z}_2\omega_2^2(1+\mu) - \tilde{Z}_1\omega_1^2 = -F_0/m_1. \tag{B.2}$$

Solving these equations give

$$\tilde{Z}_1 = \tilde{X}_1 = \frac{F_0}{m_1} \cdot \frac{-\omega^2 + \omega_2^2}{\omega^4 - \left\{\omega_2^2(1+\mu) + \omega_1^2\right\}\omega^2 + \omega_1^2\omega_2^2}, \tag{B.3}$$

$$\tilde{Z}_2 = \frac{F_0}{m_1} \cdot \frac{\omega^2}{\omega^4 - \left\{\omega_2^2(1+\mu) + \omega_1^2\right\}\omega^2 + \omega_1^2\omega_2^2}, \tag{B.4}$$

$$\tilde{X}_2 = \frac{F_0}{m_1} \cdot \frac{\omega_2^2}{\omega^4 - \left\{\omega_2^2(1+\mu) + \omega_1^2\right\}\omega^2 + \omega_1^2\omega_2^2}, \tag{B.5}$$

or more conveniently

$$\frac{\tilde{Z}_1 k_1}{F_0} = \frac{-\left(\frac{\omega}{\omega_1}\right)^2 + \frac{1}{\mu}\frac{k_2}{k_1}}{\left(\frac{\omega}{\omega_1}\right)^4 - \left\{1 + (1+\frac{1}{\mu})\frac{k_2}{k_1}\right\}\left(\frac{\omega}{\omega_1}\right)^2 + \frac{1}{\mu}\frac{k_2}{k_1}}, \tag{B.6}$$

$$\frac{\tilde{Z}_2 k_1}{F_0} = \frac{\left(\frac{\omega}{\omega_1}\right)^2}{\left(\frac{\omega}{\omega_1}\right)^4 - \left\{1 + (1+\frac{1}{\mu})\frac{k_2}{k_1}\right\}\left(\frac{\omega}{\omega_1}\right)^2 + \frac{1}{\mu}\frac{k_2}{k_1}}, \tag{B.7}$$

$$\frac{\tilde{X}_2 k_1}{F_0} = \frac{\frac{1}{\mu}\frac{k_2}{k_1}}{\left(\frac{\omega}{\omega_1}\right)^4 - \left\{1 + (1+\frac{1}{\mu})\frac{k_2}{k_1}\right\}\left(\frac{\omega}{\omega_1}\right)^2 + \frac{1}{\mu}\frac{k_2}{k_1}}. \tag{B.8}$$

We write up the characteristic equation since it will be useful later

$$\omega^4 - \left\{\omega_2^2(1+\mu) + \omega_1^2\right\} + \omega_1^2\omega_2^2 = 0, \quad \text{also written} \tag{B.9}$$

$$\left(\frac{\omega}{\omega_1}\right)^4 - \left\{1 + (1+\frac{1}{\mu})\frac{k_2}{k_1}\right\}\left(\frac{\omega}{\omega_1}\right)^2 + \frac{1}{\mu}\frac{k_2}{k_1} = 0, \quad \text{or} \tag{B.10}$$

$$\left(\frac{\omega}{\omega_2}\right)^4 - \left\{1 + \mu\left(1 + \frac{k_1}{k_2}\right)\right\}\left(\frac{\omega}{\omega_2}\right)^2 + \mu\frac{k_1}{k_2} = 0. \tag{B.11}$$

Now let the forcing frequency $\omega \to \omega_2$, with $k_1 \neq 0$ and $F_0 \neq 0$, it follows from (B.6) that

$$\tilde{Z}_1 \to 0.$$

The motion of mass m_1 approaches zero. For the mass m_2, equation (B.7) gives

$$\tilde{X}_2 \to -\frac{F_0}{m_1}\frac{1}{\mu\omega_2^2} = -\frac{F_0}{k_2}.$$

We see that m_2 moves in counter face relative to the force $F_0 e^{i\omega t}$. The force in the spring k_2 is $F = k_2 x = -F_0 e^{i\omega t}$ which is opposite in phase to the force $F_0 e^{i\omega t}$. The case is well suited for testing the numerical code for the 2DOF system. It is interesting to study the dynamic behavior of the vibration absorber as an initial value problem.

C nDOF equations for support motion

The nDOF system with base excitation can be written

$$
\begin{aligned}
m_1\ddot{x}_1 &= -k_1(x_1 - y) - c_1(\dot{x}_1 - \dot{y}) + k_2(x_2 - x_1) + c_2(\dot{x}_2 - \dot{x}_1),\\
m_2\ddot{x}_2 &= -k_2(x_2 - x_1) - c_2(\dot{x}_2 - \dot{x}_1) + k_3(x_3 - x_2) + c_2(\dot{x}_3 - \dot{x}_2),\\
&\vdots\\
m_{n-1}\ddot{x}_{n-1} &= -k_{n-1}(x_{n-1} - x_{n-2}) - c_{n-1}(\dot{x}_{n-1} - \dot{x}_{n-2}) + k_n(x_n - x_{n-1}) + c_n(\dot{x}_n - \dot{x}_{n-1}),\\
m_n\ddot{x}_n &= -k_n(x_n - x_{n-1}) - c_n(\dot{x}_n - \dot{x}_{n-1}).
\end{aligned}
$$

With $\mu_{n(n-1)} = m_n/m_{n-1}$, $z_n = x_n - x_{n-1}$, $x_0 = y$, we have for $n \geq 2$

$$
\begin{aligned}
&\ddot{z}_1 + 2\zeta_1\omega_1\dot{z}_1 + \omega_1^2 z_1 - 2\zeta_2\omega_2\mu_{21}\dot{z}_2 - \omega_2^2\mu_{21}z_2 = -\ddot{y},\\
&\ddot{z}_2 + 2\zeta_2\omega_2(1+\mu_{21})\dot{z}_2 + \omega_2^2(1+\mu_{21})z_2 - 2\zeta_1\omega_1\dot{z}_1 - \omega_1^2 z_1 - 2\zeta_3\omega_3\mu_{32}\dot{z}_3 - \omega_3^2\mu_{32}z_3 = 0,\\
&\vdots\\
&\ddot{z}_{n-1} + 2\zeta_{n-1}\omega_{n-1}(1+\mu_{(n-1)(n-2)})\dot{z}_{n-1} + \omega_{n-1}^2(1+\mu_{(n-1)(n-2)})z_{n-1} -\\
&\qquad 2\zeta_{n-2}\omega_{n-2}\dot{z}_{n-2} - \omega_{n-2}^2 z_{n-2} - 2\zeta_n\omega_n\mu_{n(n-1)}\dot{z}_n - \omega_n^2\mu_{n(n-1)}z_n = 0,\\
&\ddot{z}_n + 2\zeta_n\omega_n(1+\mu_{n(n-1)})\dot{z}_n + \omega_n^2(1+\mu_{n(n-1)})z_n - 2\zeta_{n-1}\omega_{n-1}\dot{z}_{n-1} - \omega_{n-1}^2 z_{n-1} = 0.
\end{aligned}
$$

The accelerations become

$$
\begin{aligned}
\ddot{x}_1 &= -2\zeta_1\omega_1\dot{z}_1 - \omega_1^2 z_1 + 2\zeta_2\omega_2\mu_{21}\dot{z}_2 + \omega_2^2\mu_{21}z_2,\\
\ddot{x}_2 &= -2\zeta_2\omega_2\dot{z}_2 - \omega_2^2 z_2 + 2\zeta_3\omega_3\mu_{32}\dot{z}_3 + \omega_3^2\mu_{32}z_3,\\
&\vdots\\
\ddot{x}_{n-1} &= -2\zeta_{n-1}\omega_{n-1}\dot{z}_{n-1} - \omega_{n-1}^2 z_{n-1} + 2\zeta_n\omega_n\mu_{n(n-1)}\dot{z}_n + \omega_n^2\mu_{n(n-1)}z_n,\\
\ddot{x}_n &= -2\zeta_n\omega_n\dot{z}_n - \omega_n^2 z_n.
\end{aligned}
$$

Example, the 3DOF system

$$
\begin{aligned}
&\ddot{z}_1 + 2\zeta_1\omega_1\dot{z}_1 + \omega_1^2 z_1 - 2\zeta_2\omega_2\mu_{21}\dot{z}_2 - \omega_2^2\mu_{21}z_2 = -\ddot{y},\\
&\ddot{z}_2 + 2\zeta_2\omega_2(1+\mu_{21})\dot{z}_2 + \omega_2^2(1+\mu_{21})z_2 - 2\zeta_1\omega_1\dot{z}_1 - \omega_1^2 z_1 - 2\zeta_3\omega_3\mu_{32}\dot{z}_3 - \omega_3^2\mu_{32}z_3 = 0,\\
&\ddot{z}_3 + 2\zeta_3\omega_3(1+\mu_{32})\dot{z}_3 + \omega_3^2(1+\mu_{32})z_3 - 2\zeta_2\omega_2\dot{z}_2 - \omega_2^2 z_2 = 0,\\
&\ddot{x}_1 = -2\zeta_1\omega_1\dot{z}_1 - \omega_1^2 z_1 + 2\zeta_2\omega_2\mu_{21}\dot{z}_2 + \omega_2^2\mu_{21}z_2,\\
&\ddot{x}_2 = -2\zeta_2\omega_2\dot{z}_2 - \omega_2^2 z_2 + 2\zeta_3\omega_3\mu_{32}\dot{z}_3 + \omega_3^2\mu_{32}z_3,\\
&\ddot{x}_3 = -2\zeta_3\omega_3\dot{z}_3 - \omega_3^2 z_3.
\end{aligned}
$$

Written in matrix form for implementation as a system of first order ODEs we write $\dot{X} = A_n X + Y$,

with $\dot{z}_i = \xi_i$, where

$$X = \begin{pmatrix} \xi_1 \\ z_1 \\ \xi_2 \\ z_2 \\ \vdots \\ \xi_{n-1} \\ z_{n-1} \\ \xi_n \\ z_n \end{pmatrix} \quad Y = \begin{pmatrix} -\ddot{y} \\ 0 \\ 0 \\ 0 \\ \vdots \\ 0 \\ 0 \\ 0 \\ 0 \end{pmatrix},$$

and the matrix A_n becomes for $n = 2, 3, 4$

$$\begin{pmatrix} -2\zeta_1\omega_1 & -\omega_1^2 & 2\zeta_2\omega_2\mu_{21} & \omega_2^2\mu_{21} \\ 1 & 0 & 0 & 0 \\ 2\zeta_1\omega_1 & \omega_1^2 & -2\zeta_2\omega_2(1+\mu_{21}) & -\omega_2^2(1+\mu_{21}) \\ 0 & 0 & 1 & 0 \end{pmatrix}, \tag{C.1}$$

$$\begin{pmatrix} -2\zeta_1\omega_1 & -\omega_1^2 & 2\zeta_2\omega_2\mu_{21} & \omega_2^2\mu_{21} & 0 & 0 \\ 1 & 0 & 0 & 0 & 0 & 0 \\ 2\zeta_1\omega_1 & \omega_1^2 & -2\zeta_2\omega_2(1+\mu_{21}) & -\omega_2^2(1+\mu_{21}) & 2\zeta_3\omega_3\mu_{32} & \omega_3^2\mu_{32} \\ 0 & 0 & 1 & 0 & 0 & 0 \\ 0 & 0 & 2\zeta_2\omega_2 & \omega_2^2 & -2\zeta_3\omega_3(1+\mu_{32}) & -\omega_3^2(1+\mu_{32}) \\ 0 & 0 & 0 & 0 & 1 & 0 \end{pmatrix}, \tag{C.2}$$

$$\begin{pmatrix} -2\zeta_1\omega_1 & -\omega_1^2 & 2\zeta_2\omega_2\mu_{21} & \omega_2^2\mu_{21} & 0 & 0 & 0 & 0 \\ 1 & 0 & 0 & 0 & 0 & 0 & 0 & 0 \\ 2\zeta_1\omega_1 & \omega_1^2 & -2\zeta_2\omega_2(1+\mu_{21}) & -\omega_2^2(1+\mu_{21}) & 2\zeta_3\omega_3\mu_{32} & \omega_3^2\mu_{32} & 0 & 0 \\ 0 & 0 & 1 & 0 & 0 & 0 & 0 & 0 \\ 0 & 0 & 2\zeta_2\omega_2 & \omega_2^2 & -2\zeta_3\omega_3(1+\mu_{32}) & -\omega_3^2(1+\mu_{32}) & 2\zeta_4\omega_4\mu_{43} & \omega_4^2\mu_{43} \\ 0 & 0 & 0 & 0 & 1 & 0 & 0 & 0 \\ 0 & 0 & 0 & 0 & 2\zeta_3\omega_3 & \omega_3^2 & -2\zeta_4\omega_4(1+\mu_{43}) & -\omega_4^2(1+\mu_{43}) \\ 0 & 0 & 0 & 0 & 0 & 0 & 1 & 0 \end{pmatrix}. \tag{C.3}$$

Systems with n-degrees of freedom are discussed in Thomson and Dahleh [21], chapter 6. Introducing the eigen vector matrix $(\Phi) = (\{\phi_1\}, \{\phi_2\}, \ldots, \{\phi_n\})$, the physical coordinate accelerations can be expressed in terms of the modal coordinates and the participation factor P_i, following Alexander [2]

$$\{\ddot{Z}\} = \{\phi_1\}P_1\ddot{x}_1 + \{\phi_2\}P_2\ddot{x}_2 + + \ldots + \{\phi_n\}P_n\ddot{x}_n.$$

If the modal coordinate accelerations are replaced with the absolute values of their maxima, then

$$\{\ddot{Z}\} \leq \sum_{i=1}^{n} |\{\phi_i\}P_i|\ddot{x}|\max|.$$

Since all modal maxima does not occur at the same time, the max acceleration of the j'th mass is obtained as

$$\ddot{Z}_j \max = \sqrt{\sum_{i=1}^{n} \left(\{\phi_{ij}\}P_i|\ddot{x}|\max\right)^2},$$

demonstrating that mode superposition related to the shock response spectrum is a good estimate of the maximum dynamic response.

D Analysis of 2DOF eigen frequencies

Assume $\alpha = \omega_2/\omega_1 \geq 1$ and $\mu = m_2/m_1 \geq 0$. Consider equation 3.10 and write $D = (1-\alpha)^2 + (2 + 2\alpha + \mu\alpha)\mu\alpha$.

$(\omega^*/\omega_1)^2$ is real since:

$$(1-\alpha)^2 + (2 + 2\alpha + \mu\alpha)\mu\alpha \geq 0.$$

Next show that $(\omega^*/\omega_1)^2 \geq 0$:
Must show that $(\omega_1^*/\omega_1)^2 \geq 0$. Assume contrary, then

$$\begin{aligned}
0 &> 2(\omega_1^*/\omega_1)^2, \\
&\Downarrow \\
1 + (1+\mu)\alpha &< \sqrt{D}, \\
&\Downarrow \\
1 + 2(1+mu)\alpha + (1 + 2\mu + \mu^2)\alpha^2 &< 1 - 2\alpha + \alpha^2 + 2\mu\alpha + 2\mu\alpha^2 + \mu^2\alpha^2, \\
&\Downarrow \\
2\alpha &< -2\alpha, \quad \Rightarrow \quad \alpha < 0,
\end{aligned}$$

which is a contradiction.
Finally show that $(\omega_1^*/\omega_1)^2 \leq 1$:
Assuming contrary that $(\omega_1^*/\omega_1)^2 > 1$, then

$$\begin{aligned}
1 + (1+\mu)\alpha - \sqrt{D} &> 2, \\
&\Downarrow \\
\alpha - 1 + \mu\alpha &> \sqrt{D}, \\
&\Downarrow \\
(\alpha-1)^2 + 2(\alpha-1)\mu\alpha + \mu\alpha &> (1-\alpha)^2 + 2\mu\alpha + 2\mu\alpha^2 + \mu^2\alpha^2, \\
&\Downarrow \\
-2\alpha\mu &> 2\alpha\mu, \quad \Rightarrow \alpha < 0,
\end{aligned}$$

which is a contradiction.

We have shown that ω_1^* is real and that $\omega_1^* < \omega_1$.

E Matlab example:

Plotting analytical solution for double half-sine pulse

```
function ddxdouble(per);
%    calculating acceleration of test oscillator,
%    analytic solution
%  use: ddxdouble(per)
%  input:
%    per - period of the un-damepd test oscillator
% constants
  omega = 2*pi/per;
  t1=0.01;
  t2=0.05;
  t3=0.1;
  A1 = 100;
  A2 = -A1*t1/(t2-t1);
  p1=pi/t1;
  p2=pi/(t2-t1);
  R1 = p1/omega;
  R2 = p2/omega;
  K1 = 1/(1-R1^2);
  K2 = 1/(1-R2^2);
  q = t1/(t2-t1);
%   useful arrays
  ts1 = linspace(0.0,t1,500);
  ts2 = linspace(t1,t2,2000);
  ts3 = linspace(t2,t3,2500);
  ddx1 = -A1*K1*(R1*sin(omega*ts1) - sin(p1*ts1));
%   plotting double half-sine
  figure(1)
  clf(1)
  plot(ts1,A1*sin((pi/t1)*ts1),'b')
  hold on
  plot(ts2,A2*sin((pi/(t2-t1))*(ts2-t1)),'r')
  plot(ts3,0*sin((pi/(t2-t1))*(ts3-t2)),'b')
  st1 = ['SRS input, A_1=',num2str(A1),' A_2=',num2str(A2)];
  st2 = [' t_1=',num2str(t1),' t_2=',num2str(t2)];
  title([st1,st2])
  xlabel('Time s')
  ylabel('Support acceleration m/s^2')
%  ploting solution, the un-damped oscillator of
%  period per
  figure(2)
  clf(2)
  plot(ts1,ddx1,'b')
  dum = K1*R1*sin(omega*ts2) + K2*q*sin(p2*(ts2-t1));
  ddx2 = -A1*((K1*R1 - K2*R2*q)*sin(omega*(ts2-t1)) + dum);
  hold on
  plot(ts2,ddx2,'r')

  A=(K1*R1-K2*R2*q)*cos(omega*(t2-t1))+K1*R1*cos(omega*t2)-K2*R2*q;
  B=(K1*R1-K2*R2*q)*sin(omega*(t2-t1)) + K1*R1*sin(omega*t2);
  ddx3 = -A1*(A*sin(omega*(ts3-t2))+B*cos(omega*(ts3-t2)));

  plot(ts3,ddx3,'b')
  title(['Undamped test oscillator, frequency=',num2str(1/per),' Hz'])
  xlabel('Time s')
  ylabel('ddx: Acceleration m/s^2')
```

Calculating SRS of a sDOF system

```
function SRSprod()
% use: SRSprod();
% integrating damped oscillator equation for a set of natural frequencies
% with input \ddot{y}, double half-sine pulse
  A1 = 2250;   %amplitude of support forcing displacement m/s^2
               %   A1 = 200;
  t1 = 0.0029; %duration of first half sin for the support
               %  t1 = 0.02;
  t2 = 0.0116; % endtime of second pulse
               %  t2 = 0.08;
  T2 = t2-t1;% T2 = 0.0087, duration of second half-pulse
  A2 = -(t1/(t2-t1))*A1;
  T3 = 4*t2;      % duration of sustain
  t3 = t2+T3; % = 5*t2 time for pulse + sustain
  A3 = 0;
%
  Q=5;
  zeta1 = 1/(2*Q);
  Q=10;
  zeta2 = 1/(2*Q);
  Q=100;
  zeta3 = 1/(2*Q);

  g=10.0;
% init condition t=0
  z0 = [0 0]; % [\dot{z} z] at t=0
  tspan = linspace(0.0,t3,4000);
% pulse
  figure(1)
  clf(1)
  for i=1:4000
      if tspan(i) < t1
          base(i) = A1*sin(pi*tspan(i)/t1);
      elseif (t1 < tspan(i)) && (tspan(i) < t2)
          base(i) = A2*sin(pi*(tspan(i)-t1)/(t2-t1));
      else
      base(i) = 0;
      end
  end
  plot(tspan,base)
% RK45 integration
  figure(2)
  clf(2)
  to = 1;
  for i=1:20
    to = sqrt(2)*to;
    ff(i) = 1.25*to;
    disp(['i=',num2str(i),' to=',num2str(to),...
          ' Freq =',num2str(ff(i)),'Hz'])
    omega=(2*pi)*ff(i);
    [tt1,z1]=ode45(@(tt1,z1) ddz(tt1,z1,zeta1,...
                                 omega,A1,A2,t1,t2),
                                    tspan,z0);
    [tt2,z2]=ode45(@(tt2,z2) ddz(tt2,z2,zeta2,...
                                 omega,A1,A2,t1,t2),
                                    tspan,z0);
    [tt3,z3]=ode45(@(tt3,z3) ddz(tt3,z3,zeta3,...
                                 omega,A1,A2,t1,t2),
                                    tspan,z0);
    ddx1 = -2*zeta1*omega*z1(:,1)...
           -omega*omega*z1(:,2);
    ddx2 = -2*zeta2*omega*z2(:,1)...
           -omega*omega*z2(:,2);
    ddx3 = -2*zeta3*omega*z3(:,1)...
           -omega*omega*z3(:,2);
    ddxmax1(i) = max(abs(ddx1));
    ddxmax2(i) = max(abs(ddx2));
    ddxmax3(i) = max(abs(ddx3));
    plot(tt1,ddx1)
    hold on
    plot(tt2,ddx2)
    plot(tt3,ddx3)
  end
  xlabel('t')
  ylabel('Acceleration ddx')
  %
  figure(3)
  clf(3)
  loglog(ff,ddxmax1/g,'b')
  hold on
  loglog(ff,ddxmax2/g,'r')
  loglog(ff,ddxmax3/g,'g')
  mstring = [' A_1=',num2str(A1/g),'g',' A_2=',
        num2str(A2/g),'g'];
  pstring = [' t_1=',num2str(t1),' t_2=',num2str(t2)
        ];
  s0 = strcat(mstring,pstring);
  s1 = 'SRS of double half-sine pulse';
  title({s1,s0})
  xlabel('Frequency Hz')
  ylabel('Acceleration g')
  xlim([3 5.0e+3])
  legend('Q=5','Q=10','Q=100','Location','northwest')
  grid on
%
  pseudo1 = ddxmax1./(2*pi*ff);
  pseudo2 = ddxmax2./(2*pi*ff);
  pseudo3 = ddxmax3./(2*pi*ff);
  figure(4)
  clf(4)
  loglog(ff,pseudo1,'b')
  hold on
  loglog(ff,pseudo2,'r')
  loglog(ff,pseudo3,'g')
  title({s1,s0})
  xlabel('Frequency Hz')
  ylabel('Pseudovelocity m/s')
  xlim([3 5.0e+3])
  ylim([0.1 10])
  legend('Q=5','Q=10','Q=100')
  grid on

  figure(5)
  clf(5)
  psdisp1 = pseudo1./(2*pi*ff);
  psdisp2 = pseudo2./(2*pi*ff);
  psdisp3 = pseudo3./(2*pi*ff);
  loglog(ff,psdisp1,'b')
  hold on
  loglog(ff,psdisp2,'r')
  loglog(ff,psdisp3,'g')
  title({s1,s0})
  xlabel('Frequency Hz')
  ylabel('Pseudodisplacement m')
  legend(' Q=5','Q=10','Q=100')
  grid on

  figure(6)
  clf(6)
  plottripartite(6)
  hold on
  loglog(ff,pseudo1,'b')
  loglog(ff,pseudo2,'r')
  loglog(ff,pseudo3,'g')
  title({s1,s0})
% max values of acc, pseudovel and pseudodisp
  a0 = A1;
  v0 = 2*A1*t1/pi;
  y0 = A1*t1*t2/pi;
  display(['a0,v0,y0=',num2str(a0),', ',...
           num2str(v0),', ',num2str(y0)])
  loglog([3 28 86 1280],...
  [0.024*2*pi*3 v0 a0/(2*pi*86) a0/(2*pi*1280)],'k')
```

RK45 used to integrate the equations numerically:

```
function dd = ddz(t,z,zeta,omega,A1,A2,t1,t2)
% evaluate the damped oscillator support motion equation with input
% A1,A2,t1 and t2 that defines the double half-sine support motion pulse
  dd = zeros(2,1);
  if t<t1
    dd(1) = -2*zeta*omega*z(1)-omega*omega*z(2)-A1*sin((pi/t1)*t);
  elseif (t1 < t) && (t < t2)
    dd(1) = -2*zeta*omega*z(1)-omega*omega*z(2)-A2*sin((pi/(t2-t1))*(t-t1));
  else
    dd(1) = -2*zeta*omega*z(1)-omega*omega*z(2);
  end
  dd(2)=z(1);
```

Routine used to plot tripartite mesh:

```
function plottripartite(fig)
% plotting tripartite mesh

figure(fig)
clf(fig)

g=9.81;
flow = 1.0; % frequency interval flow - fhigh
fhigh=2000;
vlow = 0.1; %velocity interval vlow - vhigh
vhigh=10;

x=flow:1:fhigh;
kk=100000;
% drawing acceleration and displacement coordinate lines
for i=1:9
    kk = kk/10;
    disp(['kk= ',num2str(kk)])
    %     mlines(kk,x,g)
    for k = kk:kk:kk*10
        f1 = log(k/(2*pi))-log(x);
        y1 = exp(f1);
        loglog(x,y1,'Color',[0.7,0.7,0.7])
        hold on
        f2 = log(k*2*pi/g)+log(x);
        y2 = exp(f2);
        loglog(x,y2,'Color',[0.7,0.7,0.7])
    end
end

% labels on coordinate lines
%  text(0.5,0.3,'0.1g')
text(1.6,1.0,'1g/0.1m')
text(5.0,3.1,'10g')
text(17,10,'100g')
text(60,32,'1000g')
%
text(60,0.03,'0.0001m')
text(17,0.10,'0.001m')
text(5.3,0.32,'0.01m')
%  text(0.5,3.1,'1m')
text(pi/2,0.09,'\pi/2')

p1 =[pi/2 pi/2]; %matching at f=\pi/2 is OK draw line to show
p2 =[1e-4 1e+2];
%loglog(p1,p2,'k')
axis([flow fhigh vlow vhigh])
grid on
xlabel(' Frequency Hz')
ylabel(' Pseudo velocity m/s')
```

References

[1] A catalogue of shock testing capabilities within STSCS nations. NATO, 2014. AC/141 (SDCG) STSCS. On Ship Combat Survivability.

[2] J. E. Alexander. Shock response spectrum - a primer. *Sound & Vibration*, pages 6–14, June 2009.

[3] J. E. Alexander. Damped 2DOF model of MIL-S-901D. medium-weight shock machine test. *Sound & Vibration*, pages 7–13, November 2016.

[4] M. A. Biot. Theory of elastic systems vibrating under transient impulse with an application to eaqrthquake-proof buildings. *Proceedings of the National Academy of Sciences*, 19(2):262–268, 1933.

[5] M. A. Biot. Analytical and experimental methods in engineering seismology. *Proceedings of the American Society of Civil Engineers*, 68:365–409, 1942.

[6] A. Brandt. *Noise and Vibration Analysis*. Wiley, 2011. ISBN 978-0-470-74644-8.

[7] Shock resistance, rules and regulations, BV0230/D5050-0623. Bundesamt für Ausrüstung, Informationstechnik und Nutzung der Bundeswehr. Defensie Materieel Organisatie, Department Maritime Systems, 2017. NATO RESTRICTED.

[8] Hermann Frahm. Us patent 989,957, 1909.

[9] P Hagedorn and G Spelsberg-Korspeter, editors. *Active and Passive Vibration Control of Structures*, volume 558. Springer, 2014. ISBN-978-3-7091-1820-7.

[10] Cyril M. Harris, editor. *Shock & Vibration Handbook*. McGraw-Hill Book Company, third edition, 1987. ISBN 0-07-026801-0.

[11] J. P. Den Hartog. *Mechanical Vibrations*. Dover Publicaitons, inc, 1956.

[12] S. J. Hiermaier. *Structures Under Crash and Impact. Continuum Mechanics, Discretization and Experimental Characterization*. Springer, 2008. ISBN-978-0-387-73862-8.

[13] L.D. Landau and E.M. Lifshitz. *Fluid Mechanics*, volume 6 of *Course of Theoretical Physics*. Butterworth Heinemann, second edition, 1987. ISBN-0-08-033932-8.

[14] G. J. O'Hara. Effect upon shock spectra of the dynamic reaction of structures. *Experimental Mechanics*, pages 145–151, May 1961.

[15] G. J. O'Hara and P.F. Cunniff. The shock spectrum dip effect. *Journal of Sound and Vibration*, 103(3):311–321, 1985.

[16] Brad Osgood. The Fourier transform and its applications. `https://see.stanford.edu/materials/lsoftaee261/book-fall-07.pdf`. Lecture Notes.

[17] Shock design criteria for surface ships. Published by Direction of Commander, Naval Sea System Command, September 1995. NAVSEA 0908-LP-000-3010 Rev.1.

[18] G. M. Remmers, G. J. O'Hara, and P. F. Cunniff. Review: Dynamic design analysis method DDAM. *Shock and Vibration*, 3(6):461–476, 1996.

[19] C. Sisemore and V. Babuska. *The Science and Engineering of Mechanical Shock*. The Science and Engineering of Mechanical Shock. Springer, 2020. ISBN 978-3-030-12102-0.

[20] Testing of surface ship equipment on shock testing machines. NATO. STANAG 4549.

[21] W. T. Thomson and M. D. Dahleh. *Theory of Vibration with Applications*. Prentice Hall, Upper Saddle River, New Jersey 078458, 5'th ed edition, 1998. ISBN 0-13-651068-X.

[22] Peter D. Welch. The use of fast fourier transform for the estimation of power spectra: A method based on time averaging over short, modified periodograms. *IEEE Transactions on Audio and Electroacoustics*, AU-15(2):70–73, June 1967.

[23] G. B. Whitham. *Linear and Nnonlinear waves*. John Wiley & Sons, Inc, 1999. ISBN-0-471-35942-4.

About FFI

The Norwegian Defence Research Establishment (FFI) was founded 11th of April 1946. It is organised as an administrative agency subordinate to the Ministry of Defence.

FFI's MISSION

FFI is the prime institution responsible for defence related research in Norway. Its principal mission is to carry out research and development to meet the requirements of the Armed Forces. FFI has the role of chief adviser to the political and military leadership. In particular, the institute shall focus on aspects of the development in science and technology that can influence our security policy or defence planning.

FFI's VISION

FFI turns knowledge and ideas into an efficient defence.

FFI's CHARACTERISTICS

Creative, daring, broad-minded and responsible.

Om FFI

Forsvarets forskningsinstitutt ble etablert 11. april 1946. Instituttet er organisert som et forvaltningsorgan med særskilte fullmakter underlagt Forsvarsdepartementet.

FFIs FORMÅL

Forsvarets forskningsinstitutt er Forsvarets sentrale forskningsinstitusjon og har som formål å drive forskning og utvikling for Forsvarets behov. Videre er FFI rådgiver overfor Forsvarets strategiske ledelse. Spesielt skal instituttet følge opp trekk ved vitenskapelig og militærteknisk utvikling som kan påvirke forutsetningene for sikkerhetspolitikken eller forsvarsplanleggingen.

FFIs VISJON

FFI gjør kunnskap og ideer til et effektivt forsvar.

FFIs VERDIER

Skapende, drivende, vidsynt og ansvarlig.

FFI's organisation

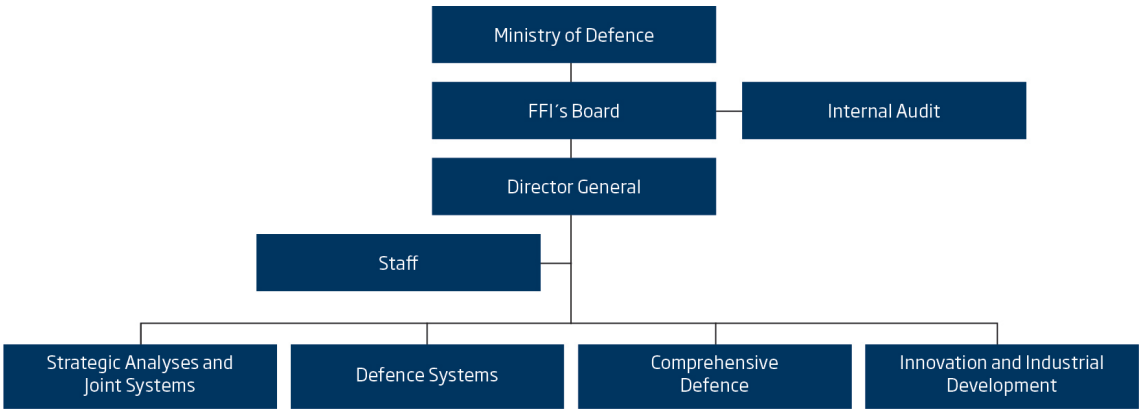

Forsvarets forskningsinstitutt
Postboks 25
2027 Kjeller

Besøksadresse:
Instituttveien 20
2007 Kjeller

Telefon: 63 80 70 00
Telefaks: 63 80 71 15
Epost: ffi@ffi.no

Norwegian Defence Research Establishment (FFI)
P.O. Box 25
NO-2027 Kjeller

Office address:
Instituttveien 20
N-2007 Kjeller

Telephone: +47 63 80 70 00
Telefax: +47 63 80 71 15
Email: ffi@ffi.no

FFI Forsvarets forskningsinstitutt
Norwegian Defence Research Establishment